

Reply to comments of Reviewer #1:

Thank you for the time and efforts you have spent on reviewing our manuscript; this is truly appreciated. Based on your comments (copied below) we reply with a point-by-point discussion of your concerns (italic and in blue color). We also include a detailed description of how we have considered your suggestions in the revised manuscript version.

General remark: Because the calibration of radiation sensors in the laboratory and the required transfer of the calibration into the field by secondary standards cause additional uncertainties of the measured irradiances and the derived layer properties, we decided to use an in-flight calibration technique (instead of relying on the laboratory calibration and its uncertain transfer to the field) for the irradiance measurements. The in-flight calibration method was already successfully applied in previous field campaigns. It is based on radiative transfer simulations of the downward irradiance in clearly cloudless sky conditions at high altitudes. In this case the measurements are only slightly affected by the atmospheric layer above the sensor and the measurements can be adjusted directly to the simulations. This in-flight calibration approach is then transferred to all radiation sensors installed in the aircraft and AIRTOSS. We have applied this calibration and concentrate on a specific measurement of the flight of 30 August 2013, which is more appropriate than the example discussed in the previous manuscript version. This specific case is characterized by a relatively high optical thickness of the cirrus layer taken into account that the vertical separation between the aircraft and AIRTOSS is 200 meters only. Another criterion for selecting this measurement case was that there was no additional cirrus above or below the layer enclosed by the aircraft and AIRTOSS. So we have chosen a case most suitable to derive optical layer properties of cirrus.

The following figure shows the new measurement case from 30 August 2013, measured above the North Sea.

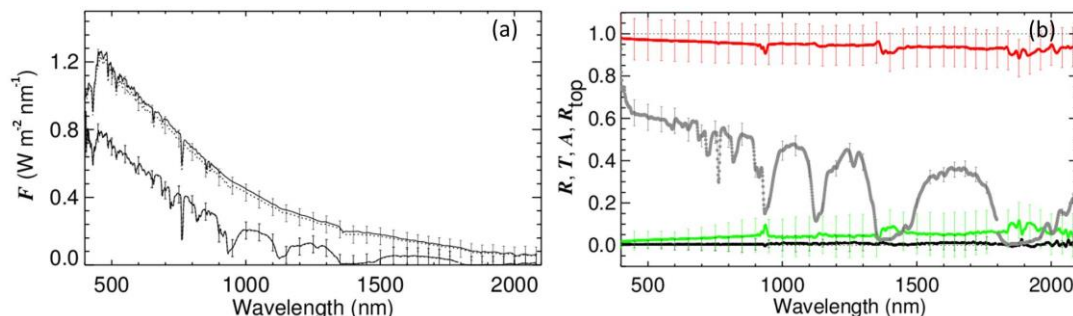


Fig.7: (a) shows measured spectral downward and upward irradiance F from the aircraft above the cloud layer (solid lines) and AIRTOSS below the cloud layer (dotted lines) at the time, indicated by the vertical dashed line in Fig 1. F_{top} is simulated. (b) shows spectral reflectivity (black), transmissivity (red), absorptivity (green), and cloud top albedo (gray) according to irradiance in (a). The vertical bars indicate the systematic errors due to measurement uncertainties.

Reviewer #1: Abstract Line 18-21:

Mention the optical thickness of the low level cloud and say that the found differences in cirrus properties are only true for a low level cloud with these properties. Maybe add how an optically thicker/thinner and geometrically lower/higher low cloud changes the found impact.

Reply: We have followed your advice and included a new Fig. 13, which shows the influence of the optical thickness of the underlying liquid water cloud and the cloud top height on the broadband radiative forcing of the cirrus, for different cirrus optical thickness values. This clearly quantifies the effect of low liquid water clouds on the cirrus radiative forcing.

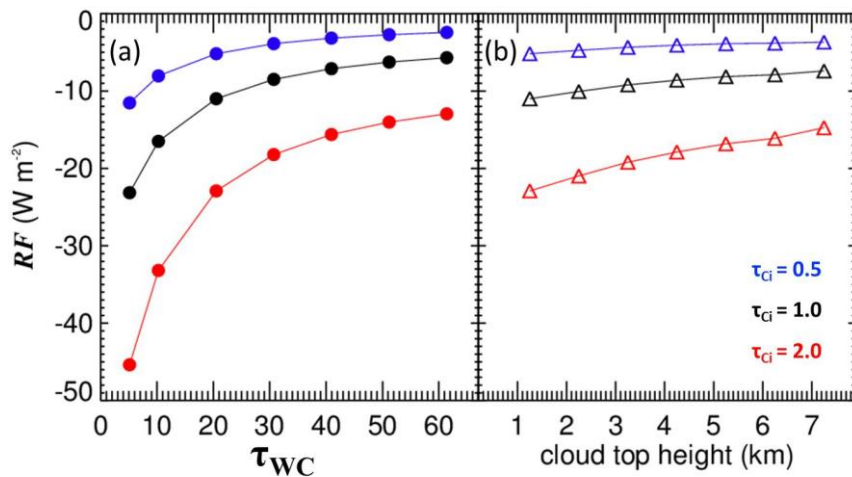


Fig. 13: Integrated values of cirrus radiative forcing when a low water cloud is present. The optical thickness (left panel), and the top height (right panel) of the water cloud are varied. The colors indicate a different cirrus optical thickness.

“The results obtained in this paper are valid for the respective cloud cases. To evaluate the low-level cloud effect on the cirrus the properties of the low water cloud, such as optical thickness and cloud top height, have to be investigated, too. Therefore, Fig. 13 (a) and (b) show values of integrated cirrus radiative forcings (wavelength range: 300–2300 nm) with varying water cloud optical thickness (a) and cloud top height (b). The cirrus is located between 6.7 km and 8.5 km altitude and consists of the mixture of shapes according to Baum et al. (2005). The color code represents the changing cirrus optical thickness.

In Fig.13 (a) the low-level cloud is located between 1 km and 1.25 km with an increasing optical thickness from 5 to 60. In general, the cooling of the cirrus decreases with increasing optical thickness of the low cloud resulting in an increasing influence of the low cloud on the upper lying cirrus. This is due to the reflected radiation by the low cloud being available to interact with the cirrus layer again. With higher water cloud optical thickness a saturating effect can be seen resulting in differences of 72% to 83%. Additionally, with increasing cirrus optical thickness the absolute difference of RF increases from 10Wm^{-2} to 32Wm^{-2} .

In Fig.13 (b) the low water cloud has a constant optical thickness of 20, and a vertical thickness of 250m with an increasing cloud top height from 1.25 to 7.25 km. Similar to Fig.13 (a) the cooling of the cirrus decreases with increasing cloud top height of the low-level cloud. Here, the amount of the reflected radiation by the low cloud, available in the cirrus level, depends on the vertical extension of the atmosphere in between and its interaction with the transmitted (from cirrus) and reflected (from water cloud) radiation. The trend of RF is similar to (a) with increasing cloud top height with a resulting in lower differences of 20% to 35% and absolute values of not more than 8Wm^{-2} . It is noticeable that the cloud optical thickness of the low cloud in comparison to the cloud top height has a significant effect on the radiative forcing of the above lying cirrus.”

Reviewer #1: p.19047 Line 10ff:

Cirrus inhomogeneities are described in the motivation – where do you analyze their impact on layer properties? Regarding p.19047 Line 15ff: Here you describe impact of ice crystal size and shape on remote sensing retrievals – make extra paragraph to distinguish from impact of cirrus inhomogeneities.

Reply: *Spatial inhomogeneities of the microphysical cirrus properties, such as ice crystal shape, size and number concentration, result in spatially varying optical properties of the cirrus. The spatial variability of the microphysical properties is presented in Figure 5. The impact of these microphysical and optical cirrus parameters, that represent the cloud*

inhomogeneities, is investigated. As an example, Figure 11 illustrates the impact of different ice crystal shapes on both the optical cirrus layer properties and the cirrus radiative forcing. In Figure 10 the size distribution effect on the cirrus optical layer properties and its radiative forcing is quantified. What has not been done is to directly link the spatial variability of the microphysical/optical cirrus properties with optical layer properties and the radiative forcing. That would require to think about the need to consider three-dimensional radiative effects, which would go beyond the scope of this paper.

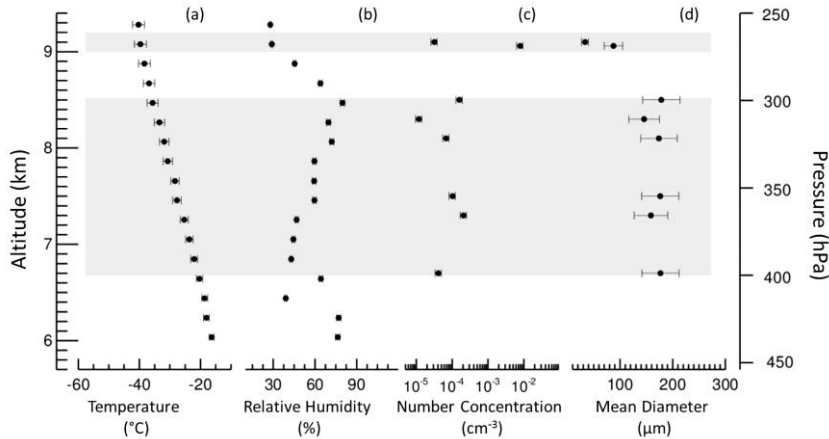


Fig. 5: Vertical profiles of (a) temperature, (b) relative humidity, measured on the Learjet 35A, (c) number concentration, and (d) mean diameter, derived by CIPg on AIRTOSS, from the flight of 30 August 2013. The bars show the corresponding measurement uncertainties. The gray area indicates the vertical extent of the cirrus layer.

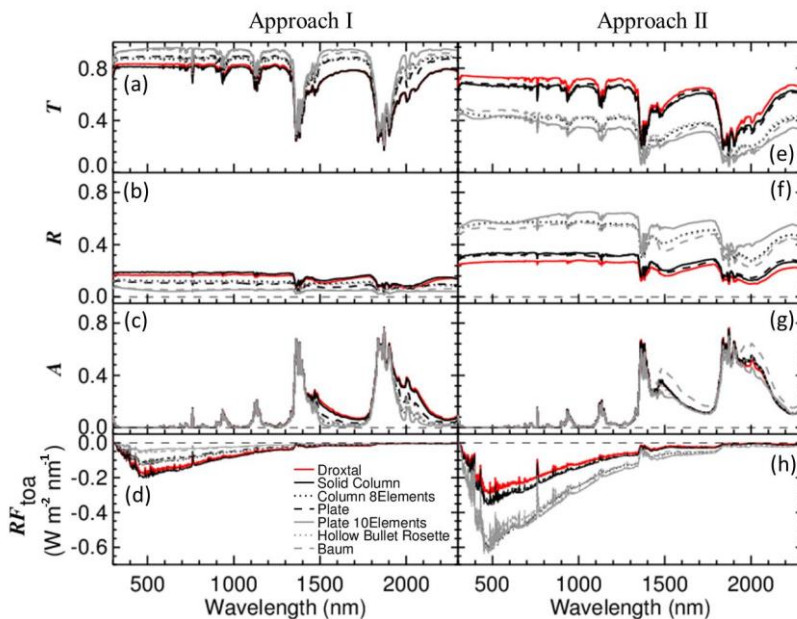


Fig. 11: Shown are spectral (a,e) transmissivity, (b,f) reflectivity, and (c,g) absorptivity of a cirrus layer between 6.7 and 8.5 km altitude. (e,h) are the radiative forcings at TOA, respectively. The simulations are based on a measured number size distribution assuming different ice particle shapes. The two panels indicate two conditions: constant number size distribution (Approach I) and constant ice water content (Approach II).

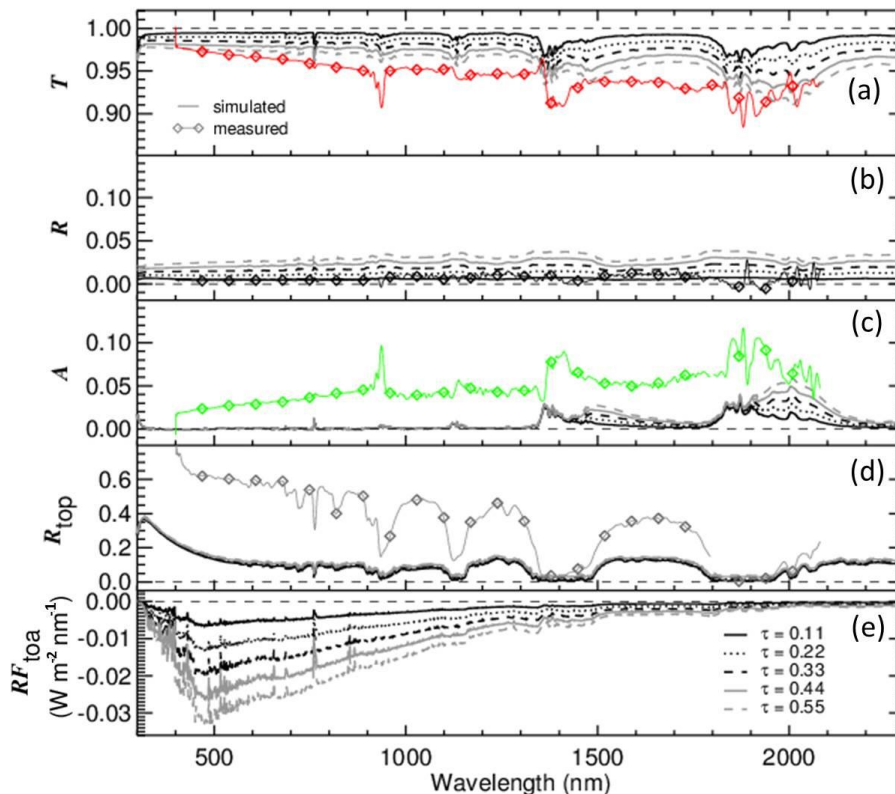


Figure 10. The lines show simulated, spectral (a) transmissivity, (b) reflectivity, and (c) absorptivity of a cirrus layer between 9 km and 9.2 km altitude. (e) are the radiative forcings at TOA, respectively. The simulations are based on a measured number size distribution assuming the mixture of shapes according Baum et al. (2005). Inserted is the measurement case (diamonds) from Fig.7.

Reviewer #1: p.19048 Line 10:

If I understand correctly, you are presenting the first collocated spectral radiation measurements above and below cirrus with a towing sonde to derive optical layer properties here? – Highlight here that this is the new contribution of this paper!

Reply: Thank you for this advice! We have highlighted this crucial point of the paper in both the abstract and the conclusions of the paper.

“Spectral solar optical layer properties of cirrus are derived from simultaneous and vertically collocated measurements of spectral upward and downward solar irradiances above and below the cirrus layer. From the irradiance data spectral transmissivity, absorptivity, reflectivity, and cloud top albedo of the observed cirrus layer are obtained. The radiation measurements are supplemented by in-situ microphysical measurements and radiative transfer simulations based on the microphysical data.”

Reviewer #1: p.19049 Line 7ff:

Explain why you assure horizontal stabilization of the irradiance sensor mounted on top of the aircraft to measure downwelling irradiances but not of the sensor measuring upward irradiances mounted on the wingpod.

Reply: The horizontal stabilization of the upward looking optical inlet is important to assure appropriate measurement data, especially due to the direct portion of the downward radiation. In contrast, the upward radiation consists of a larger amount of diffuse radiation being less influenced by the orientation of the sensor. An active horizontal levelling of all

irradiance sensors would be desirable, however, from a technical point of view this is illusionary, and from a scientific perspective it is crucial only for the downward irradiance measurement, which has a major direct component, whereas the other sensor have mostly receive diffuse radiation, which is much less sensitive to horizontal sensor misalignments.

Reviewer #1: p.19053 Line 8ff:

Describe Fig.6 more in detail – strong variations of mean particle diameter are obvious, comment on them, they represent cloud inhomogeneities.

Reply: *Thank you for this hint. But for the new measurement example, showing very low number concentrations and a well-mixed cirrus cloud layer, we decided not to show this figure.*

Reviewer #1: p.19058 Line 1:

Explain why you choose this measured particle number size distribution and not a different one.

Reply: *The chosen number size distribution, measured by the microphysical sensors, installed in the AIRTOSS sensor platform, is considered to represent a cirrus cloud typical for the measurement case investigated in the paper. This has been shown by looking at time series of the size distribution measurements. If integrated, it eventually leads to an optical thickness of 1, typical for the investigated cirrus.*

Reviewer #1: p.19058 Line 26:

Radiative forcing of Solid Columns and Droxtals is strongest (not lowest!), they exhibit the strongest negative forcing. Be careful in describing your results properly.

Reply: *Thank you for reading that careful, we apologize for this misprint.*

Reviewer #1: p.19060 Line 2:

Choosing a water cloud with $\tau = 45$ at 1.5-1.75km comes a bit out of the blue. Where do you take those values from? A 250m thick water cloud with $\tau = 45$ seems unrealistic.

Reply: *This is a valid point. We have changed the properties of the low liquid water cloud to an optical thickness of 20 and an altitude range from 1 to 1.25 km. We base these assumptions on concurrent satellite data of MODIS. The corresponding text has been revised and a further investigation of the impact of the low-level cloud properties optical thickness and cloud top height is presented in Section 5.3 of the manuscript (see Fig. 13).*

Reviewer #1: p.19060 Line 21f:

Clarify that the “overestimation of the cooling effect of the cirrus” refers to the single-layer cirrus case. How often do we have conditions of cirrus with underlying clouds? – Quantify. Also comment on if previous studies in which cirrus radiative forcing was estimated paid attention to single-layer only cirrus or if they potentially overestimated the cooling effect by not excluding multi-layer conditions.

Reply: *Chang and Li (2005) have reported in their climatology of single-layered and overlapped clouds an annual and global occurrence of high clouds of 52 – 61 % (ocean – land) from which 27 % to 29 % represent cases with low clouds underneath the cirrus. Thus these low clouds beneath cirrus represent a significant portion. This quantitative information is now given in the text of the revised manuscript.*

„Chang and Li (2005) reported an annual and global occurrence of high clouds of 52 – 61% (ocean – land), from which 27% to 29% represent cases with low clouds underneath the cirrus. During the flights very often low clouds were observed, that is why the related effect of a low-level water cloud was investigated.“

Chang, F.-L., Li, Z.: A Near-Global Climatology of Single-Layer and Overlapped Clouds and Their Optical Properties Retrieved from Terra/MODIS Data Using a New Algorithm, J. of Climate, 18, 4752–4771, 2005

Reply to comments of Reviewer #2:

Thank you for the time and efforts you have spent on reviewing our manuscript; this is truly appreciated. Based on your comments (copied below) we reply with a point-by-point discussion of your concerns (italic, in blue). We also include a detailed description of how we have considered your suggestions in the revised manuscript version.

General remark: Because the calibration of radiation sensors in the laboratory and the required transfer of the calibration into the field by secondary standards cause additional uncertainties of the measured irradiances and the derived layer properties, we decided to use an in-flight calibration technique (instead of relying on the laboratory calibration and its uncertain transfer to the field) for the irradiance measurements. The in-flight calibration method was already successfully applied in previous field campaigns. It is based on radiative transfer simulations of the downward irradiance in clearly cloudless sky conditions at high altitudes. In this case the measurements are only slightly affected by the atmospheric layer above the sensor and the measurements can be adjusted directly to the simulations. This in-flight calibration approach is then transferred to all radiation sensors installed in the aircraft and AIRTOSS. We have applied this calibration and concentrate on a specific measurement of the flight of 30 August 2013, which is more appropriate than the example discussed in the previous manuscript version. This specific case is characterized by a relatively high optical thickness of the cirrus layer taken into account that the vertical separation between the aircraft and AIRTOSS is 200 meters only. Another criterion for selecting this measurement case was that there was no additional cirrus above or below the layer enclosed by the aircraft and AIRTOSS. So we have chosen a case most suitable to derive optical layer properties of cirrus.

Reviewer #2: Experimental Setup: Figure 7: From grey shaded area in this plot (and Figure 5), the cirrus layer would extend beyond 1 km depth. The described experiment, where the AIRTOSS was extended a distance of 900 m (185 m vertical), would not provide collocated radiation measurements above and below the cirrus layer.

Reply: You are correct, sorry for the confusion we caused here. This has not been described adequately in the manuscript. As the vertical difference between the two platforms is not more than about 200 m the investigated cloud layer, shown by the measurements in Fig. (7) and (8), represents a part of the complete cirrus layer. The revised sketch in Fig. (3) attempts a more clear explanation of the selection of the measurement case.

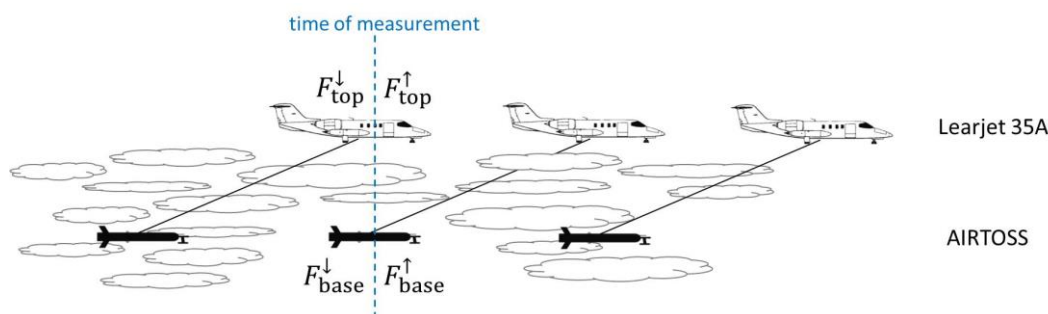


Fig. 3: Schematic sketch of measurement setup to measure collocated upward and downward irradiance at two altitudes.

Reviewer #2: In the region prior to that marked I and II, spaced by approximately 100 seconds of flight, was the AIRTOSS lowered even further? If it was not, then much of the supporting points given to support the use of AIRTOSS below and aircraft above (both of which were instrumented with radiation measurements), would describe a theoretical approach – not one that was enacted in practice. This should be made clear, and the title of the manuscript (“: : a feasibility study: : ” should be revised).

Reply: Thank you for the advice! The manuscript title has been changed to “Spectral Optical Properties of Cirrus from Collocated Measurements and Simulations”.

We carefully screened the entire data set and selected a new measurement case (see Fig. 7) for the revised manuscript version. It represents a cirrus layer, that was directly between the two measurement platforms aircraft and AIRTOSS, thus not more than 200 m in vertical extent, which enables to measure above and below this cirrus layer.

Another reason is, that above and below the cirrus no additional cirrus layer was present during this part of the measurement flight.

Furthermore, this cirrus layer has a higher optical thickness compared to other measurement cases. Therefore, it shows even for the vertical extent of 200 m measurable and visible differences between the measured spectral irradiances.

Reviewer #2: In addition, ancillary support (microphysical data, other data?) for the region I as cloud free below cirrus, and region II as low-cloud below cirrus, is not given in the manuscript text. This would be an important point to address, given that an assumption of the analysis is that there is zero horizontal divergence of radiation – either within the cirrus layer or from high to low optical depth of the underlying (water) cloud. On this note, the assumption of zero horizontal divergence could be better established in the text.

Reply: The new measurement example, as well as the complete measurement flight of 30 August, was influenced by a low – level cloud layer. This is supported by a video (recorded out of the cockpit) as well as synoptic forecast and MODIS data (see Fig. 4). That is why Fig. 7 shows one measurement example, with a low – level water cloud.

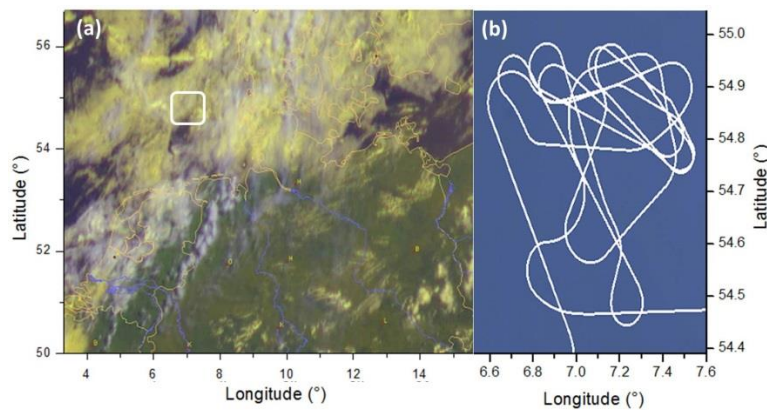


Fig. 4: (a) Composite satellite image of the cloud situation on 30 August 2013 at 9:45 UTC showing cirrus (white) above yellow colored lower water clouds (DeutscherWetterdienst / EUMETSAT).



Picture from out of the cockpit of the Learjet, showing the cloud situation during the flight. The low-level cloud layer is visible with the cirrus cloud above.

The assumption of neglecting horizontal components of radiative flux divergences in our approach was explicitly included in the revised manuscript version just after Equation 3, where we now state: “Eq. 3 implicitly assumes that there are no horizontal components of radiative flux divergence, only vertical flux divergences are considered to derive absorptivity.”

Reviewer #2: Please also note that the level of the cirrus cloud was given different values in the manuscript (please check for consistency).

Reply: *Okay, sorry for this error, which has been removed in the revised manuscript version.*

Reviewer #2: Deriving Cloud layer optical properties from collocated measurements: Figure 8: As best I can gather, the downwelling irradiance above the cirrus layer came from a model, and not measurements. (In most spaces in text and captions, it is identified as a measurement, but in others, it is identified as model results). Besides the fact that it is unclear why a model has been used (given the discussion on a leveling platform in the manuscript), it must be considered that a mismatch between the measured and modeled downwelling irradiation above the cirrus layer would propagate into all of the derived quantities shown in the right hand plots. This mismatch would be an additional source of error that would propagate into the derived quantities because deriving these layer quantities is already subject to large systematic errors, given that the reflectivity and absorptivity are small values derived from differences in large irradiances. For example, the absorptivity results (subplots c and d) at wavelengths < 900 nm (i.e., conservative scattering wavelengths), show non-zero absorption when single scattering albedo at these wavelengths is essentially unity and true cloud absorption is expected to be zero. To achieve (expected) zero absorptivity results at these spectral bands would require error bars that are 2-3X or more larger than the stated 5-6% uncertainty. Since the results of Figure 8 are (largely) derived only from measurements (the exception being the downwelling irradiance above cloud), I would ask for a comparison of measured and modeled downwelling irradiance above the cloud, and a percentage difference value between them.

Reply: *There were some temporal problems with the active levelling of the optical inlet measuring the downward irradiance on the Learjet during the campaign. Therefore we have replaced the measured downward irradiances (Learjet) by respective simulations whenever the leveling platform did not work appropriately. That is well justified in case of measurements at high altitudes with no cirrus above. We have proven in numerous field campaigns that for such cases the horizontally levelled measurements are accurately described by simulations. This is not in contradiction with the general need to apply levelling platforms for measurements under more complicated cloud situations, which we avoided in the manuscript by carefully choosing a case with no cirrus above the high measurement altitude.*

Reviewer #2: I would also argue that the upwelling irradiances below the cirrus base (subplot a) is larger than what would be expected for over-ocean, clear-sky measurements. What is the justification that low-level clouds were absent— what ancillary measurements did you use? And, how robust is the statement without support from lidar measurements, for example?

Reply: *We have carefully screened all data available and on this basis have chosen a specific flight sequence, which is well appropriate to derive the cirrus layer properties. Finding such cases is not as easy as it appears from a first glance. As a result we came up with a new measurement case that we have investigated in detail. The new measurement example, as well as the complete measurement flight of 30 August, was influenced by a low-level cloud layer. The problem you have seen in the previous manuscript version does not appear anymore, mostly because the effects caused by the low-level liquid water cloud.*

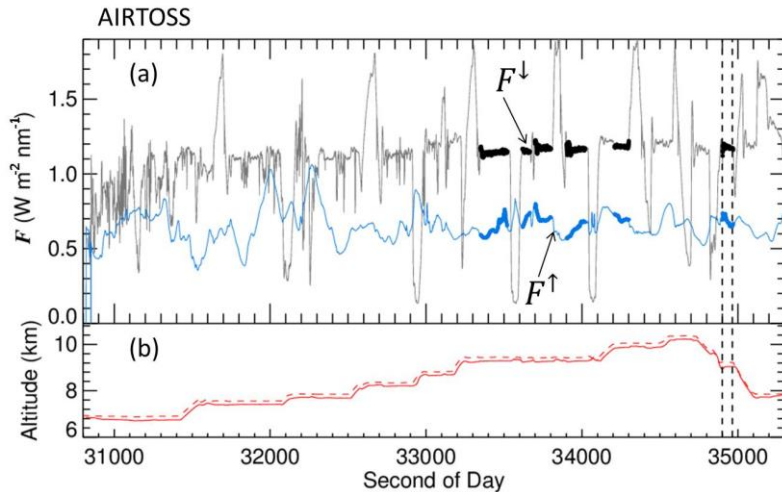


Fig.6: (a) Time series of downward (gray) and upward (light blue) irradiance F ($\text{Wm}^{-2} \text{nm}^{-1}$) measured on AIRTOSS at one wavelength (550 nm) from the flight of 30 August 2013. The thickened line periods mark the measuring points at straight flight legs. The red lines in (b) show the altitude of AIRTOSS (solid) and Learjet (dashed). The vertical dashed line marks the measurement example in Fig. 2.

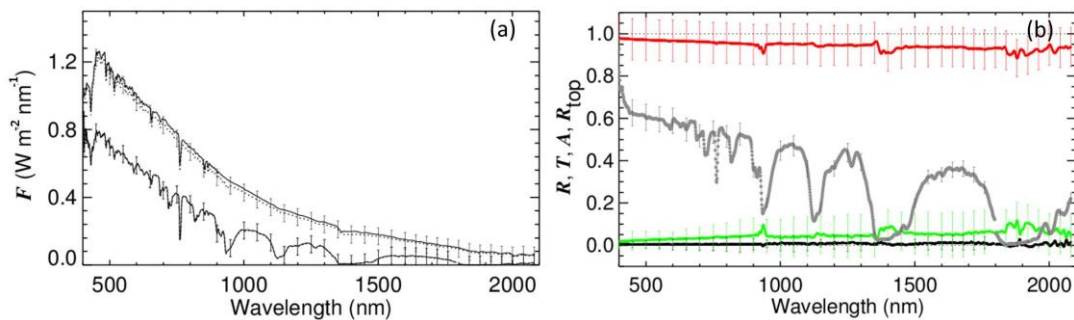


Fig.7: (a) shows measured spectral downward and upward irradiance F from the aircraft above the cloud layer (solid lines) and AIRTOSS below the cloud layer (dotted lines) at the time, indicated by the vertical dashed line in Fig 1. F_{top} is simulated. (b) shows spectral reflectivity (black), transmissivity (red), absorptivity (green), and cloud top albedo (gray) according to irradiance in (a). The vertical bars indicate the systematic errors due to measurement uncertainties.

Reviewer #2: Finally, given that the underlying surface albedo is ocean (in the absence of low-level cloud), I would ask that authors please remove all statements suggesting that variability in the cirrus reflectance is due to changing ground conditions given that ocean albedo is dark (low albedo) and relatively flat, spectrally.

Reply: Thank you for the advice! Please, see answers above relating the measurement example and the conditions below the investigated cirrus. We removed the statements criticized by the reviewer.

Reviewer #2: Comparing Measurements with Simulations: Please ensure that you make clear that the use of 1-D RT simulations will not capture horizontal radiation motion, potentially biasing your results (relative to “truth”, as represented in a model by 3-D). Section 5.1: RT simulations – This section really needs more description to understand, with any certainty, the approach that has been applied. However, I believe this has been the general approach:

a) An (equivalent) particle diameter in conjunction with model single scattering properties and measured number size distribution, to compute bulk, volumetric layer properties. What were the assumptions to go from the non-spherical crystal shape to equivalent particle diameter?

Note also that the equations 7-9 should be revised to “dlogD” to correspond with the measurements in Figure 6.

Reply: *The equivalent particle diameter (effective particle size) is defined as the ratio between the volume of the particle $V(L)$ and the projected area $A(L)$, where L is the maximum dimension of the nonspherical particle. A detailed explanation is given by Yang et al., 2005.*

Yang, P., Wei, H. L., Huang, H. L., Baum, B. A., Hu, Y. X., Kattawar, G. W., Mishchenko, M. I., and Fu, Q.: Scattering and absorption property database for nonspherical ice particles in the near- through far-infrared spectral region, Appl. Opt., 44, 5512–5523, 2005.

Reviewer #2: b) The results from a) were used to model cloud optical properties, tau and reff. c) Derived tau and reff are then used to model upwelling and downwelling irradiance at cloud top and cloud bottom. d) Cloud layer properties are then derived from the irradiances computed in c). e) To investigate the cloud layer properties and cloud radiative forcing for different assumptions in crystal shape and habit mixture, a fixed number size distribution is combined with different shape assumptions.

Reply: *Thank you for making this point. We have extended the explanation of our approach in the revised manuscript version. As you described correctly, the measured number size distribution is used to compute the volumetric optical properties. These bulk properties, e.g., extinction coefficient and phase function, serve as input for the radiative transfer model to derive the upward and downward irradiances at two altitudes, top and bottom of the cirrus. In turn the irradiances are used to calculate the layer properties transmissivity, reflectivity, and absorptivity, and the radiative forcing of the cirrus layer. By leaving the size distribution constant the ice crystal shape is varied to investigate its effect. In the revised manuscript version we have added a second scenario, which seems physically even more plausible. In this second approach we have kept the ice water content constant. For both scenarios we have investigated effects of changing ice crystal shape in detail. The description of the two approaches has been given in detail in the revised manuscript version.*

Reviewer #2: One of my concerns with the results is focused on Figure 10 (albedo panel): None of the simulations, irrespective of crystal habit, reproduce the measured cloud top albedo. If I have understood the experimental process described above in points a-d, the failure to reproduce cloud top albedo calls into the interpretation of the layer properties and the cloud radiative forcing results.

Reply: *The cloud top albedo is a measure of the optical properties of the complete atmospheric layer and the surface below. So, the properties of the low cloud influence the cloud top albedo as well and can only be reproduced poorly by the simulations due to a lack of knowledge about the lower cloud layer.*

Reviewer #2: There are two, additional, key variables that are necessary to understand the results, that are I do not believe are provided in the manuscript: approximate optical thickness of the cirrus cloud, and solar zenith angle. For optically thin clouds, single scattering will dominate and assumptions in crystal shape will be emphasized (as opposed to an optically thicker cloud where multiple reflections smooths out some of the differences due to crystal shape/habit assumptions). In addition for low sun angles, multiple scattering will also be emphasized.

Reply: *Your statements are correct, the degree of multiple scattering determines the magnitude of crystal shape effects. This is true in spectral regions with insignificant absorption, whereas in absorption bands multiple scattering amplifies shape effects. However, in this manuscript the focus is not to evaluate these dependencies by numerous sensitivity tests. Instead we take the measurements we have and try to come up with a consistent picture of the cirrus optical layer properties and related radiative effects for a specific measurement case, for which we have as many reliable measurements as possible. Then we investigate the effect of ice crystal shapes in Fig. 11 and for varying optical*

thickness in Fig. 10, where different number size distributions are assumed, which mimics variations of cirrus optical thickness. We have not looked at the effects of different solar zenith angles, instead we have used the actual values during the measurements, which did not vary more than about 4 degrees.

Reviewer #2: Interpreting conclusions related to Changing Crystal Shape/Habit: I feel holding the number size distribution constant is an inadequate approach to quantifying differences in cloud layer properties. Understanding differences in cloud radiative forcing due to crystal shape and/or habit changes would require an approach that enforced constant IWC;

Reply: Thank you for the advice. As mentioned above we have added the scenario with a variable IWC into the revised manuscript. Please find the according layer properties and cirrus radiative forcing spectra in Figs. 10 (e) – (h). A respective discussion has been added to the text of the revised manuscript.

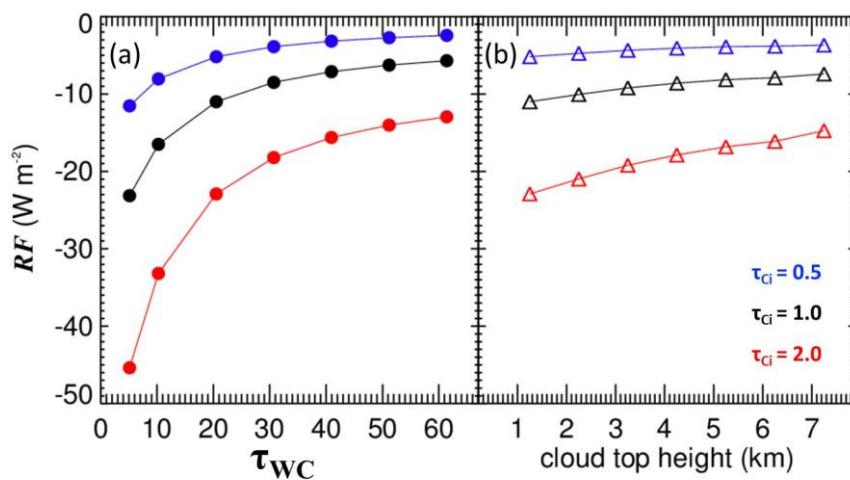


Fig. 13: Integrated values of cirrus radiative forcing when a low water cloud is present. The optical thickness (left panel), and the top height (right panel) of the water cloud are varied. The colors indicate a different cirrus optical thickness.

“The results obtained in this paper are valid for the respective cloud cases. To evaluate the low-level cloud effect on the cirrus the properties of the low water cloud, such as optical thickness and cloud top height, have to be investigated, too. Therefore, Fig. 13 (a) and (b) show values of integrated cirrus radiative forcings (wavelength range: 300–2300 nm) with varying water cloud optical thickness (a) and cloud top height (b). The cirrus is located between 6.7 km and 8.5 km altitude and consists of the mixture of shapes according to Baum et al. (2005). The color code represents the changing cirrus optical thickness.

In Fig.13 (a) the low-level cloud is located between 1 km and 1.25 km with an increasing optical thickness from 5 to 60. In general, the cooling of the cirrus decreases with increasing optical thickness of the low cloud resulting in an increasing influence of the low cloud on the upper lying cirrus. This is due to the reflected radiation by the low cloud being available to interact with the cirrus layer again. With higher water cloud optical thickness a saturating effect can be seen resulting in differences of 72% to 83%. Additionally, with increasing cirrus optical thickness the absolute difference of RF increases from 10Wm^{-2} to 32Wm^{-2} .

In Fig.13 (b) the low water cloud has a constant optical thickness of 20, and a vertical thickness of 250m with an increasing cloud top height from 1.25 to 7.25 km. Similar to Fig.13 (a) the cooling of the cirrus decreases with increasing cloud top height of the low-level cloud. Here, the amount of the reflected radiation by the low cloud, available in the cirrus level, depends on the vertical extension of the atmosphere in between and its interaction with the transmitted (from cirrus) and reflected (from water cloud) radiation. The trend of RF is similar

to (a) with increasing cloud top height with a resulting in lower differences of 20% to 35% and absolute values of not more than 8Wm^{-2} . It is noticeable that the cloud optical thickness of the low cloud in comparison to the cloud top height has a significant effect on the radiative forcing of the above lying cirrus.”

Reviewer #2: ... holding IWC constant was the approach also used by studies cited in this manuscript [Zhang et al., 1999] or to provide another boundary condition to results achieve by holding number size distribution constant [Wendisch et al., 2007]. To support the analysis results, plots of the spectral volumetric extinction coefficient, and single scattering albedo (as a function of crystal shape/habit, for perhaps 1-2 different particle diameters) should also be shown. The authors could also show the derived asymmetry parameter (first moment of the scattering phase function) as well.

Reply: We prefer not to add further graphs showing volumetric optical properties, this is beyond the focus of our manuscript. Instead we concentrate on the cirrus layer optical properties, resulting from measurement (microphysical) based simulations, and compare them with concurrent radiation measurements. We hope you will accept this decision.

The approach of assuming a constant ice water content, showing a more physical approach, was added to the simulations. In Fig. 11 different assumptions of ice crystal shape are investigated for the two approaches (I: constant number size distribution, II: constant IWC).

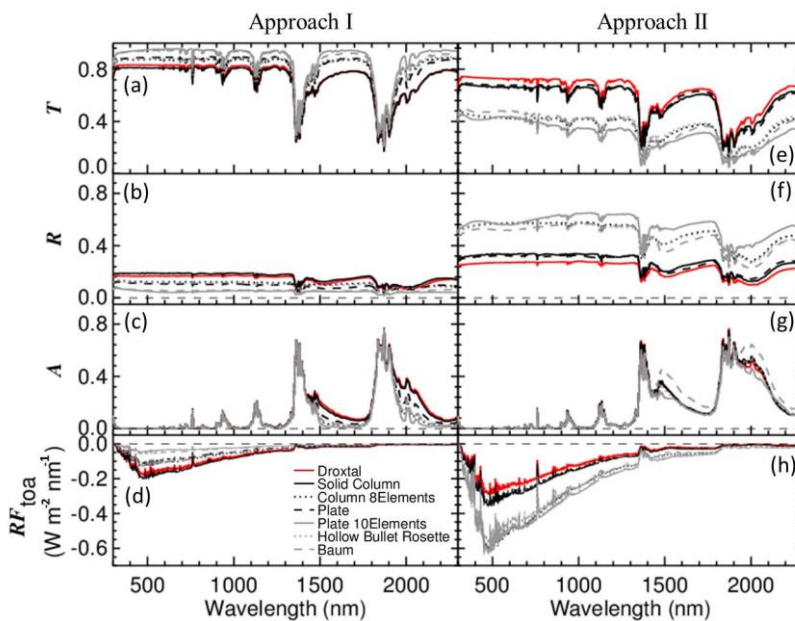


Fig. 11: Shown are spectral (a,e) transmissivity, (b,f) reflectivity, and (c,g) absorptivity of a cirrus layer between 6.7 and 8.5 km altitude. (e,h) are the radiative forcings at TOA, respectively. The simulations are based on a measured number size distribution assuming different ice particle shapes. The two panels indicate two conditions: constant number size distribution (Approach I) and constant ice water content (Approach II).

Reply to comments of Reviewer #3:

Thank you for the time and efforts you have spent on reviewing our manuscript; this is truly appreciated. Based on your comments (copied below) we reply with a point-by-point discussion of your concerns (italic, in blue). We also include a detailed description of how we have considered your suggestions in the revised manuscript version.

General remark: Because the calibration of radiation sensors in the laboratory and the required transfer of the calibration into the field by secondary standards cause additional uncertainties of the measured irradiances and the derived layer properties, we decided to use an in-flight calibration technique (instead of relying on the laboratory calibration and its uncertain transfer to the field) for the irradiance measurements. The in-flight calibration method was already successfully applied in previous field campaigns. It is based on radiative transfer simulations of the downward irradiance in clearly cloudless sky conditions at high altitudes. In this case the measurements are only slightly affected by the atmospheric layer above the sensor and the measurements can be adjusted directly to the simulations. This in-flight calibration approach is then transferred to all radiation sensors installed in the aircraft and AIRTOSS. We have applied this calibration and concentrate on a specific measurement of the flight of 30 August 2013, which is more appropriate than the example discussed in the previous manuscript version. This specific case is characterized by a relatively high optical thickness of the cirrus layer taken into account that the vertical separation between the aircraft and AIRTOSS is 200 meters only. Another criterion for selecting this measurement case was that there was no additional cirrus above or below the layer enclosed by the aircraft and AIRTOSS. So we have chosen a case most suitable to derive optical layer properties of cirrus.

Reviewer #3: The measurement of cloud layers properties from collocated aircraft goes back several decades and lead to the “anomalous absorption” problem. Cloud flux divergence is a difficult measurement to make under the best circumstances. The inhomogeneous and often optically thin cirrus clouds makes them especially difficult. The authors correctly point out that collocated aircraft should, in theory, lead to better estimates of cloud layer properties such as absorptance (absorptivity). But the collocation of aircraft is no guarantee that it will. The problem of horizontal flux divergence still exists and substantial errors in the results of airborne flux divergence measurements are common/expected (e.g. Schmidt et al., 2010, Marshak et al., 1999). Other authors have proposed methods to ameliorate the effects of horizontal flux divergence (Cox and Ackerman and Cox, 1981, Marshak et al., 1999), and these techniques have lead to plausible results (Kindel et al., 2011).

Reply: Thanks for this compressed summary of the problem, of course we agree. In case of optically thin cirrus the question of the importance of horizontal photon transport was one of the motivations for our study.

Reviewer #3: It is clear from the results shown in this paper that despite the collocation of the spectral irradiance measurements, there are significant problems with the measurements that are not addressed in the paper. See for instance, Figure 7. The absorptivity, shown in green, exhibits more than 10% absorption in the visible and then decreases as it approaches 1000 nm at which time it becomes negative (non-physical). The absorption of ice cloud (and liquid water cloud) is zero (single-scattering albedo is 1) for the visible wavelengths regardless of the ice particle size or shape (see Figure 7(c)). The absorption begins to decrease at the point it should begin to increase in the near-infrared. The single-scattering albedo drops below one in the near-infrared and some absorption is expected. No discussion of the significant absorption in the visible is given in the text, nor are the effects of horizontal flux divergence or any attempt to compensate for them. There is one sentence remarking on the effect of horizontal photon transport in section 4.2.2. It explains lower absorptivity in the 1000 to 1500 nm range and a result of horizontal photon transport in the cloud layer. I cannot make sense of what is meant here. Why only 1000 to 1500 nm? In the cirrus layer or the low cloud layer or both?

Reply: We carefully screened the entire data set and selected a new measurement case for discussion in this manuscript. The modified and new measurement example does not show these anomalous values anymore.

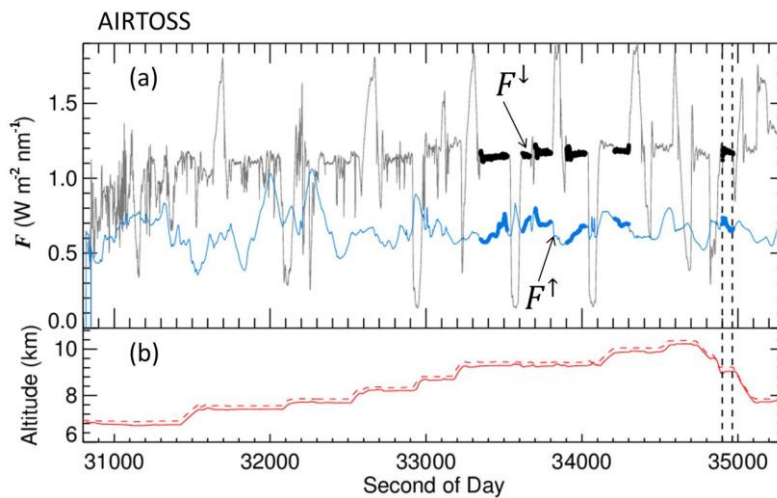


Fig.6: (a) Time series of downward (gray) and upward (light blue) irradiance F ($\text{Wm}^{-2} \text{nm}^{-1}$) measured on AIRTOSS at one wavelength (550 nm) from the flight of 30 August 2013. The thickened line periods mark the measuring points at straight flight legs. The red lines in (b) show the altitude of AIRTOSS (solid) and Learjet (dashed). The vertical dashed line marks the measurement example in Fig. 2.

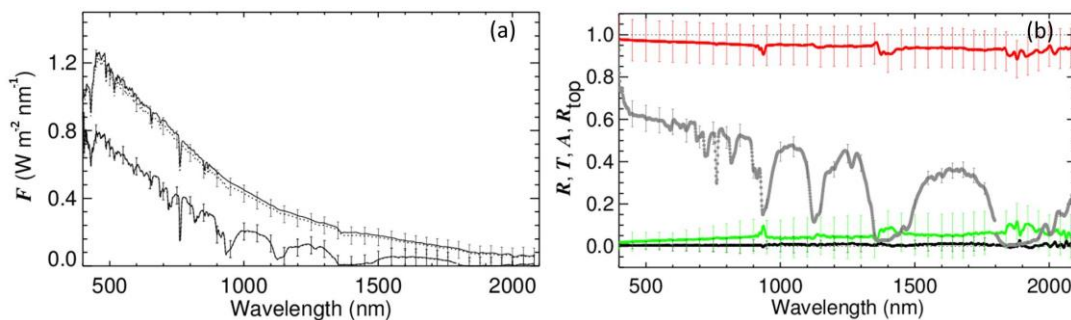


Fig.7: (a) shows measured spectral downward and upward irradiance F from the aircraft above the cloud layer (solid lines) and AIRTOSS below the cloud layer (dotted lines) at the time, indicated by the vertical dashed line in Fig 1. F_{top} is simulated. (b) shows spectral reflectivity (black), transmissivity (red), absorptivity (green), and cloud top albedo (gray) according to irradiance in (a). The vertical bars indicate the systematic errors due to measurement uncertainties.

This measurement example was chosen due to the higher optical thickness, and because of the low vertical extent, which enables to measure above and below this cirrus layer.

Reviewer #3: The measurement of reflectivity has an unusual shape as well. The reflectance goes up in the near infrared (Figure 10(b)). This is not what is expected nor is it what is demonstrated in the modeling. Reflectance goes down in the near infrared for a cloud over a dark surface (in this case water). The authors, in Equation 4, point out that the sum of T , R , and A must equal one (i.e. energy conservation). Why not plot $T+R+A$?

Reply: As the cloud optical layer properties of the investigated cirrus are derived by using the equations (1)-(3) including the measured upward and downward irradiances, equation (4) shows that the sum of the three quantities always holds unity. This is a matter of definition, see equation (4). This is valid for both, measurements and simulations.

Reviewer #3: This would be a good test of the validity of the measurements. This would also be a good test of the modeling results as well, which also contain results that seem to be incorrect. For instance, in Figure 12(b), R becomes negative between 1500 to 1800 nm and 2000 to 2200 nm. What is negative reflectivity? Additionally, in Figure 12(b) the water vapor absorption bands (940, 1140, 1400, and 1900 nm) have greater reflectivity than the surrounding window regions. How is this possible?

Reply: *Please see the comments above. The new measurement example does not show these anomalous values anymore.*

Reviewer #3: The modeled albedo (Figure 12(d), spectrum in black) R_{top} increases with wavelength; the albedo is greater in near-infrared than in the visible. Again, how is this possible?

Reply: *The modified and new measurement example does not show these anomalous values anymore.*

Reviewer #3: The measurement of R_{top} makes more sense than the model in this case. The albedo decreases in the infrared. Additionally, it would be very useful to list the optical thickness and effective radius along with the shape used in all the calculations given in this work.

Reply: *Thank you for the advice! A table with the listed optical thicknesses for the different ice crystal shapes can be found in the paper, now.*

Table 1: Shown are the optical thicknesses for a cirrus between 6.7 km and 8.5 km altitude assuming different ice crystal shapes for Approach I (constant number size distribution) and Approach II (constant ice water content).

	Approach I	Approach II
Droxtal	1.49	2.68
Solid Column	1.50	3.20
Column 8 Elements	0.77	7.45
Plate	1.15	4.44
Plate 10 Elements	0.54	15.4
Hollow Bullet Rosette	0.97	9.52
Baum	1.00	5.09

Reviewer #3: The differences are substantial between the shapes, but it is not clear what the differences are in the optical thicknesses and effective radii. There are aspects of the measurement technique that are unclear and confusing. The measurement, as I understand it, was made with the aircraft above the cloud layer and the AIRTOSS below the cloud layer (see Figure 3.) This is coupled with a relatively minor offset in time (5 or 6 seconds) because the AIRTOSS trails the aircraft. In Figure 7 the shaded gray area delineates the cloud vertical extent. I estimate the thickness to be about 1.7 km. In the section describing the time correction the vertical extent of the AIRTOSS from the aircraft is given as 914 meters. This, even if flown directly beneath the aircraft, is not long enough to span the thickness of the cirrus layer.

Reply: *You are correct, this has not been described adequately in the manuscript. As the vertical difference between the two platforms is not more than about 200 m the investigated cloud layer, shown by the measurements in Fig. (7) and (8), represents a part of the complete cirrus layer. The sketch in Fig. (3) shows the principle of collecting measurements when a cloud layer is in between the two platforms.*

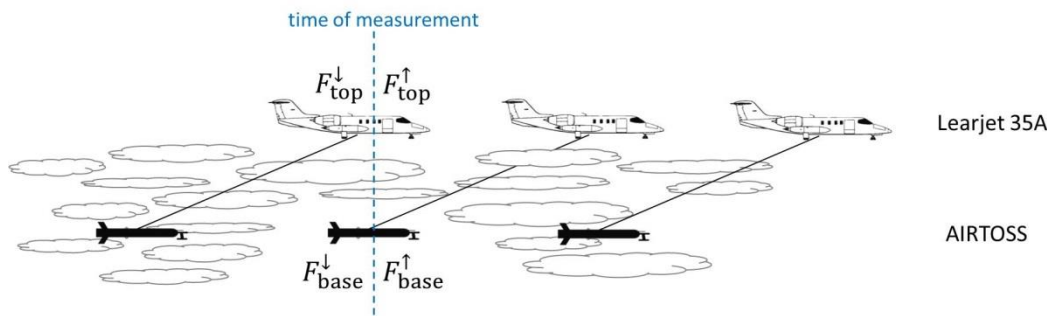


Fig. 3: Schematic sketch of measurement setup to measure collocated upward and downward irradiance at two altitudes.

Reviewer #3: Additionally, in Figure 8, the F_{down} from above the cloud layer is simulated not from the aircraft measurement. What is the point of using a model F_{down} if a measurement was made?

Reply: *There were some temporal problems with the active levelling of the optical inlet measuring the downward irradiance on the Learjet during the campaign. Therefore we have replaced the measured downward irradiances (Learjet) by respective simulations whenever the leveling platform did not work appropriately. That is well justified in case of measurements at high altitudes with no cirrus above. We have proven in numerous field campaigns that for such cases the horizontally levelled measurements are accurately described by simulations. This is not in contradiction with the general need to apply levelling platforms for measurements under more complicated cloud situations, which we avoided in the manuscript by carefully choosing a case with no cirrus above the high measurement altitude.*

Reviewer #3: This would help to offset any radiometric calibration errors if all of the spectrometers were calibrated to the same radiometric source. Why not plot the aircraft and the AIRTOSS altitude on Figure 7(b)?

Reply: *Thank you for the good advice. Please, see the two altitude curves in Fig. (1).*

Reviewer #3: It would make it clear exactly where the aircraft and AIRTOSS were during the measurement period. If the measurements were not truly collocated, that is, aircraft measured irradiances above the cloud layer, and AIRTOSS measurements below the cloud layer, measured within five or six seconds of each other, it is difficult to see how this technique differs from a single aircraft experiment.

Reply: *There are several advantages to use the setup of aircraft and towed platform in contrast to a single aircraft measurement. Firstly, in the altitude range of cirrus clouds the wind velocities are high resulting in a fast passage of the cirrus out of the measurement area. Furthermore, they might change their microphysical and optical properties during the time the second measurement can be performed. Secondly, it is hard, or nearly impossible, to assure that the field of view during the second measurement is the same as for the first. So, the setup of Learjet and AIRTOSS ensures a maximum temporal difference of 5 to 6 seconds between the measurement at two different altitudes and both devices investigate the same spatial sectors being crucial for investigating the cloud layer in between.*

Reviewer #3: The irradiance ($F_{\text{base up}}$) reported for Time I (Figure 8(a)) the “no low-level cloud” is far too high to be an irradiance spectrum over cloudless ocean. These spectra clearly include the effects of low-level cloud. Over cloudless ocean, the peak of the upwelling irradiance in the near infrared is rarely, if ever, over $0.1 \text{ (W m}^{-2} \text{ nm}^{-1}\text{)}$. Was this period of “no” low level cloud selected on the irradiance values alone or was it confirmed with ancillary data such as aircraft video?

Reply: The new measurement example, as well as the complete measurement flight of 30 August, was influenced by a low – level cloud layer. This is supported by a video (recorded out of the cockpit) as well as synoptic forecast and MODIS data (see Fig. 4).

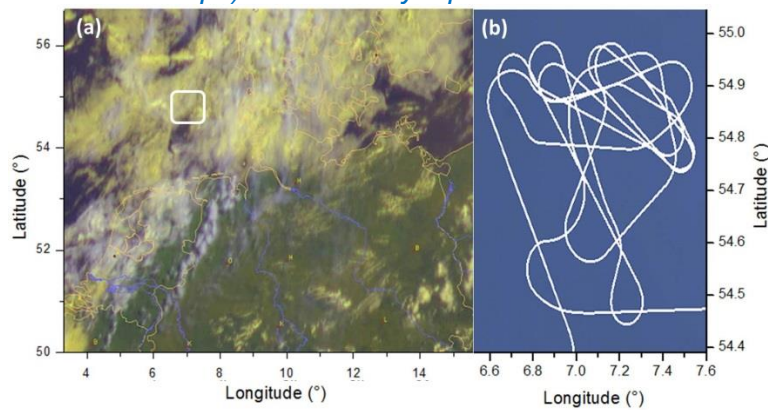


Fig. 4: (a) Composite satellite image of the cloud situation on 30 August 2013 at 9:45 UTC showing cirrus (white) above yellow colored lower water clouds (DeutscherWetterdienst / EUMETSAT).



Picture from out of the cockpit of the Learjet, showing the cloud situation during the flight. The low–level cloud layer is visible with the cirrus cloud above.

Reviewer #3: It is not clear to me why this is called a feasibility study. Generally, a feasibility study in this context is meant to denote analysis undertaken to demonstrate whether a particular measurement is likely to be successful given the characteristics of the problem and the performance of an instrument/measurement technique. This is not a feasibility study, as I understand it. Measurements were made and the results are in poor agreement with modeling results and what is generally expected from basic cloud and atmospheric radiative transfer.

Reply: Thank you for your advice! The manuscript title has been changed to “Spectral Optical Layer Properties of Cirrus from Collocated Airborne Measurements and Simulations”.

Spectral Optical Layer Properties of Cirrus from Collocated Airborne Measurements and Simulations

Fanny Finger^{1,5}, Frank Werner^{1,2}, Marcus Klingebiel³, André Ehrlich¹, Evelyn Jäkel¹, Matthias Voigt³, Stephan Borrmann^{3,4}, Peter Spichtinger³, and Manfred Wendisch¹

¹Leipzig Institute for Meteorology (LIM), University of Leipzig, Germany

²University of Maryland (UMBC), Physics Department, Baltimore, Maryland, USA

³Institute for Atmospheric Physics, Johannes Gutenberg University Mainz, Germany

⁴Max Planck Institute for Chemistry, Mainz, Germany

⁵Dr. Födisch Umweltmesstechnik AG, Markranstädt, Germany

Correspondence to: F. Finger
f.finger@uni-leipzig.de

Abstract. Spectral solar optical layer properties of cirrus are derived from simultaneous and vertically collocated measurements of spectral upward and downward solar irradiances above and below the cirrus layer. From the irradiance data spectral transmissivity, absorptivity, reflectivity, and cloud top albedo of the observed cirrus layer are obtained. The radiation measurements are supplemented by in-situ microphysical measurements and radiative transfer simulations based on the microphysical data. The close collocation of the radiative and microphysical measurements, above, beneath and inside the cirrus, is accomplished by using a research aircraft (Learjet 35A) in tandem with the towed sensor platform AIRTOSS (AIRcraft TOWed Sensor Shuttle). AIRTOSS can be released from and retracted back to the research aircraft by means of a cable up to a distance of 4 km. Data were collected in two field campaigns over the North Sea and the Baltic Sea in spring and late summer 2013. Exemplary results are discussed also to illustrate the benefits of collocated sampling. Furthermore, based on the measured cirrus microphysical properties, radiative transfer simulations were applied to quantify the impact of cloud particle properties such as crystal shape, effective radius r_{eff} , and optical thickness τ on cirrus spectral optical layer properties. The effects of clouds beneath the cirrus are evaluated. They may cause changes in both the spectral optical layer properties and the radiative forcing of the cirrus by a factor of 2. If low-level clouds below the cirrus are not taken into account the solar cooling due to the cirrus is significantly overestimated.

1 Introduction

Significant uncertainties in atmospheric and climate modelling originate from the insufficient description of effects and interactions of clouds with solar and terrestrial radiation (IPCC, 2013). In particular, cirrus clouds are critical; they mostly warm but can also cool the atmosphere, depending on cloud optical properties and altitude (Lynch et al., 2002). Cirrus clouds globally occur at all latitudes and in all seasons with a mean global coverage of about 20 – 30 %. More than 70 % of cirrus are observed in the tropics (Wylie et al., 1994), forming relatively stable and long-lived cloud layers (Liou, 1986). Due to different meteorological conditions and evolution processes cirrus clouds are characterized by a wide diversity of macrophysical structures, sizes and numbers of ice particles, crystal shapes and orientations. Horizontal and vertical inhomogeneities of these properties increase the complexity of cirrus. The radiative layer properties (reflectivity, transmissivity, and absorptivity) of cirrus depend on the microphysical (effective radius r_{eff} , ice water content IWC) and optical (absorption, scattering) characteristics.

Cirrus inhomogeneities and varying crystal shapes impact (i) the energy budget of the Earth’s atmosphere, and (ii) the remote sensing of cirrus optical thickness τ and r_{eff} , which is often based on one-dimensional (1D) radiative transfer modelling. Schlimme et al. (2005) found that the horizontal variability of the extinction coefficient leads to significant differences in the solar irradiance compared to a homogeneous cloud, resulting in a variability of transmittance of about 80 %. Zhang et al. (1999) reported that the radiative forcing of cirrus may switch sign depending on the geometry and size of the ice crystals. The impact of ice crystal shape on the cirrus radiative forcing, depending on the solar zenith angle, can vary between 10 and 26 % for the solar spectral range (Wendisch et al., 2005), while for the thermal infrared spectral range even differences of up to 70 % are found (Wendisch et al., 2007). Eichler et al. (2009) investigated the influence of ice crystal shape on the retrieval of τ and r_{eff} and reported effects of up to 70 % for τ and 20 % for r_{eff} .

Measurements of spectral layer properties of cirrus are rarely available. Commonly a combination of measurements and simulations is applied to derive layer properties, whereby τ and r_{eff} are retrieved from reflected radiance (airborne or space-borne) (see Francis et al., 1998) and then used in combination with a radiative transfer model to simulate layer reflectivity, transmissivity, and absorptivity.

Airborne measurements of cirrus optical layer properties are hard to obtain if only one aircraft is used. Usually, the radiative measurements above and below the cirrus are performed consecutively (e.g., Pilewskie and Valero, 1992). This method unavoidably involves a temporal shift between the two measurements above and below the cirrus and, thus, can be applied for rather static and horizontal homogeneous cloud layers only. Therefore, helicopter-borne towed platforms have been developed and adapted, such as the Airborne Cloud Turbulence Observation System (ACTOS) for microphysical in situ instruments, and the Spectral Modular Airborne Radiation measurements system – HELIcopter-borne Observations of Spectral Radiation (SMART-HELIOS) for solar spectral reflectivity measurements (Henrich et al., 2010; Werner et al., 2013, 2014). For cirrus measurements,

55 Frey et al. (2009) introduced the aircraft-borne AIRTOSS (AIRcraft TOWed Sensor Shuttle), shown in Fig. 1.

In this paper an extended version of AIRTOSS will be presented with additional spectral radiation sensors, which allows for the first time to derive cloud optical layer properties from truly collocated spectral upward and downward radiation measurements. In Section 2 the instrumentation of the aircraft and AIRTOSS is described. In particular, the solar spectral radiation instruments and their
60 combination to derive optical layer properties are discussed in Section 3. In Section 4 the calculated solar spectral layer properties and the concurrent microphysical observations are introduced for one exemplary measurement case. Based on these data radiative transfer simulations are performed and analyzed in Section 5.

65 **2 Instrumentation**

The instruments were mounted at different positions on the aircraft, the towed platform AIRTOSS, and an additional wing pod underneath the left wing as illustrated in Fig. 2 (a). The operation of the aircraft together with the tethered AIRTOSS is certified for altitudes up to 12.5 km (the previous ceiling limitation was 7.6 km; Frey et al., 2009).

70 **2.1 Aircraft**

The applied aircraft certified for the operation of AIRTOSS is a Learjet 35A. Instruments for measurements of trace gases and water vapor are mounted inside the cabin with special inlets sampling ambient air from outside the aircraft during the flight. An upward looking radiation sensor, measuring the downward irradiance F^\downarrow (in $\text{W m}^{-2} \text{nm}^{-1}$), was mounted on the fuselage including the
75 Spectral Modular Airborne Radiation measurement syStem (SMART) inside the aircraft, introduced by Wendisch et al. (2001), further developed by Bierwirth et al. (2009). Optical fibers connect the optical inlet with two Zeiss Spectrometers for the visible to near infrared (300 – 2200 nm) wavelength range with a resolution (Full Width at Half Maximum, FWHM) of 2 – 3 nm (visible) and 9 – 16 nm (near infrared), respectively. An active horizontal stabilization platform (Wendisch et al.,
80 2001) was operated to assure the horizontal levelling of the upward looking optical inlet on top of the aircraft during the aircraft measurements, which is crucial for unbiased irradiance measurements. A pod mounted under the left wing of the aircraft contains another optical inlet with a pair of spectrometers, measuring the upward irradiance. A Forward Scattering Spectrometer Probe (FSSP-100), placed at the tip of the wing pod, measures the cloud particle number size distribution (size diameter range from 2 to 47 μm , Gayet et al., 2002). To correct for shattering (Korolev et al., 2013) the FSSP-100 records the individual data particle-by-particle (Field et al., 2003, 2006). The instrument was used as indicator for the time periods when the aircraft was inside clouds and for estimates of general parameters like mean cloud particle diameter.

2.2 AIRTOSS

90 AIRTOSS, as shown in Fig. 2 (b), has a length of 2.85 m and a diameter of 24 cm; the maximum payload is 40 kg. It can be released from and retracted to the aircraft by a 4 km long towing cable.

In the front part of AIRTOSS the Cloud Combination Probe (CCP, see e.g., Wendisch and Brenguier, 2013; Klingebiel et al., 2015) is installed. The CCP consists of the Cloud Droplet Probe (CDP) and the Cloud Imaging Probe instrument (CIP grey scale – denoted as CIPgs in the following). The

95 CDP measurement principle is similar to the FSSP–100 and detects particles in the size diameter range between 2 μm and 50 μm by measuring the forward-scattered light of a laser beam which hits individual particles. The CIPgs records two-dimensional (2D) shadow images of the particles and covers a size range between 15 μm and 960 μm with an optical resolution of 15 μm . The performance of these microphysical cloud probes in cirrus clouds was characterized by McFarquhar et al. (2007).

100 The center part of AIRTOSS contains a battery for power supply, which is sufficient to assure electrical power for measurements of about two hours. The radiation setup is mounted in the backward part of AIRTOSS. It consists of two spectrometer pairs and two optical inlets, one upward and one downward looking, measuring the downward and upward spectral irradiance F . Additional sensors for static air temperature and relative humidity, latitude, longitude and position angles pitch, roll and
105 heading of AIRTOSS are installed.

The housing of the towed platform consists of an aerodynamic canister to avoid irregular movements and to enable quiet flying, which is crucial for reliable radiation measurements (Frey et al., 2009).

3 Optical layer properties

Four optical inlets, two for upward and two for downward irradiance measurements were mounted
110 on the Learjet 35A and AIRTOSS. This setup enabled to simultaneously measure the irradiance in two different altitudes (e.g., above and below cloud) as required to calculate cloud layer properties (see Fig. 3). By measuring the upward and downward irradiances at the top and base of a cloud layer the optical properties are derived as follows. The reflectivity R is given by:

$$R = \frac{F^{\uparrow}_{\text{top}} - F^{\uparrow}_{\text{base}}}{F^{\downarrow}_{\text{top}}}. \quad (1)$$

115 R quantifies the relative portion of incoming solar radiation that is reflected by the cloud layer. The transmissivity T of a cloud layer is defined by:

$$T = \frac{F^{\downarrow}_{\text{base}}}{F^{\downarrow}_{\text{top}}}. \quad (2)$$

It describes the part of the incoming irradiance transmitted through the cloud. The relative portion of irradiance absorbed inside the cloud layer is defined by the absorptivity:

120
$$A = \frac{(F^{\downarrow}_{\text{top}} - F^{\uparrow}_{\text{top}}) - (F^{\downarrow}_{\text{base}} - F^{\uparrow}_{\text{base}})}{F^{\downarrow}_{\text{top}}}. \quad (3)$$

Equation 3 implicitly assumes that there are no horizontal components of radiative flux divergence, only vertical flux divergences are considered to derive absorptivity. From these definitions it follows:

$$R + T + A = \frac{F^{\uparrow}_{\text{top}} - F^{\uparrow}_{\text{base}} + F^{\downarrow}_{\text{base}} + F^{\downarrow}_{\text{top}} - F^{\uparrow}_{\text{top}} - F^{\downarrow}_{\text{base}} + F^{\uparrow}_{\text{base}}}{F^{\downarrow}_{\text{top}}} = 1. \quad (4)$$

The cloud top albedo R_{top} is given by:

$$125 \quad R_{\text{top}} = \frac{F^{\uparrow}_{\text{top}}}{F^{\downarrow}_{\text{top}}}. \quad (5)$$

R_{top} describes the cloud reflection property of the cloud layers and the underlying surface. For investigating the effect of a cirrus layer on the atmospheric radiative energy budget the radiative forcing (RF_{toa}) at the top of atmosphere (toa) is used, defined by:

$$RF_{\text{toa}} = (F^{\downarrow}_{\text{toa}} - F^{\uparrow}_{\text{toa}})_{\text{cloud}} - (F^{\downarrow}_{\text{toa}} - F^{\uparrow}_{\text{toa}})_{\text{clear sky}}. \quad (6)$$

130 The subscripts "cloud" and "clear sky" indicate measurements or simulations in cloudy conditions and in a clear sky atmosphere. A positive RF_{toa} indicates a warming effect of the cloud on the underlying atmosphere and surface, whereas a negative RF_{toa} indicates a cooling effect.

4 Observations

Measurements were performed during two observational campaigns in spring (6 – 8 May) and late
 135 summer (29 August – 5 September) in 2013. The research flights were based at the military airports in Hohn and Jagel, North Germany, and were carried out in restricted flight areas above the North and Baltic Sea. The measurement areas represent boxes with the size of 50 x 80 km², and 35 x 80 km², respectively. Stepwise horizontal flight patterns were flown to collect radiative and microphysical data at different altitudes (6 – 11.5 km). The transport of tropospheric air masses into the stratosphere
 140 was reported by Mueller et al. (2015). In total, twelve measurement flights were carried out during both campaigns; four of them were analyzed in detail.

Measurements are presented of one exemplary flight which took place west of the German island of Helgoland above the North Sea (54.98° – 54.43°N, 6.59° – 7.57°E); it was performed on 30 August 2013 (08:33 – 09:48 UTC). Northern Germany was under the influence of an occluded front with
 145 associated cirrus and the center of the low south of Norway (see Fig. 4).

Fig. 4 (a) shows the corresponding composite satellite image of METEOSAT-10. In the image the high cirrus clouds are indicated by white color. Low clouds are labelled by yellow color and were present over a large area, including parts of the measurement area. The flight track of the Learjet 35A is shown in Fig. 4 (b).

150 4.1 Microphysical measurements

Fig. 5 shows the vertical profiles of (a) static air temperature (in °C), (b) relative humidity (in %) with respect to ice, measured by instruments on the aircraft, (c) number concentration (in cm⁻³), and (d)

mean diameter (in μm), measured by the CIPgs on AIRTOSS. The bars quantify the measurement errors, resulting from instrument uncertainties (a, b), counting statistics (c), and determination of the depth of field (d). Considering the measured ice particle number concentration the cirrus was identified in altitudes between 6.7 km and 8.5 km and between 9.0 km and 9.2 km, with a temperature range of -21°C to -39°C .

Fig. 5 (c) and (d) show the particle number concentration and mean diameter as a function of altitude. Each data point is a mean value for a 200 m height interval. The cirrus layer between 6.7 and 8.5 km shows values for the number concentration of $1.2 \times 10^{-4} \text{ cm}^{-3}$ to $2.1 \times 10^{-3} \text{ cm}^{-3}$ and for the mean diameter of 145.6 and 178.3 μm , representing an optically thin and vertically well mixed cirrus. The gaps of measured number concentration and mean diameter are due to measurements outside the observed cirrus. The second cirrus layer between 9.0 and 9.2 km altitude shows increased values for the number concentration of up to $7.9 \times 10^{-3} \text{ cm}^{-3}$ and lower values for the mean diameter of 33.5 to 87.4 μm . This results in an optically thicker cirrus in comparison to a 200 m thick part of the cirrus layer between 6.7 and 8.5 km altitude.

4.2 Radiation data

4.2.1 Spectral irradiances

In Fig. 6 (a) the time series of downward and upward irradiance measured by AIRTOSS at a wavelength of 550 nm is illustrated for the entire flight: gray for downward and light blue for upward irradiance. The altitude of the Learjet (dashed red line in Fig. 6 (b)) and AIRTOSS (solid red line) show the stepwise climbing flight pattern and the different altitudes of the level legs as well as the vertical distance of about 200 m between both. The gray colored peaks in the time series of the irradiance (Fig. 6 (a)) are due to flight manoeuvre and have to be excluded from further analysis. The measured pitch and roll angles of the AIRTOSS were used to sort out the data assuming a threshold of 5° . Resulting are the thickened line periods marking the measuring points at straight flight legs. The almost constant values of the downward irradiance ($1.09 - 1.20 \text{ W m}^{-2} \text{ nm}^{-1}$) are a result of the thin cirrus layer above the sensor. The upward irradiance is influenced by the surface albedo and changing conditions due to underlying clouds; they show values between 0.56 and 0.81 $\text{W m}^{-2} \text{ nm}^{-1}$ at 550 nm.

As the AIRTOSS is dragged behind the aircraft time allocation of the radiation measurements of the towed platform has to be adjusted to that measured simultaneously on the Learjet 35A to guarantee clear vertical collocation of the measurements. The temporal shift between the aircraft and AIRTOSS was calculated by using the cable length (914 m), aircraft velocity ($150 - 170 \text{ ms}^{-1}$) and altitude difference of both platforms, as a function of the true air speed. The resulting altitude and time difference varies between 160 m and 210 m, corresponding to 4.8 seconds to 6 seconds. Mean values of measured spectra of upward and downward irradiance from both platforms are shown

in Fig. 7 from the time interval, indicated by the dashed lines in Fig. 6. The investigated cirrus layer is located between 9 and 9.2 km altitude and can be seen in Fig.5 (c) and (d), indicated by the upper gray colored layer. This measurement example was chosen due to the higher optical thickness, as reported in Section 4.1, and because of the low vertical extent, which enables to measure above and below this cirrus layer.

The vertical difference between the two measurement platforms is 195 m in the specific example discussed here. The downward irradiance $F^{\downarrow}_{\text{top}}$ at the top of the cloud layer was simulated (Mayer and Kylling, 2005). The black solid lines show the irradiance, measured in the flight altitude of the Learjet above the cloud layer (subscript top), the black dotted lines represent the irradiance measured from the AIRTOSS at the base of the investigated part of the cirrus layer (subscript base).

As expected, the downward irradiance below the cirrus ($F^{\downarrow}_{\text{base}}$) is lower than that measured above the cloud ($F^{\downarrow}_{\text{top}}$). This shows that the attenuation of the solar radiation (reflection and absorption by cirrus particles) by the observed cirrus can actually be quantified by observational means. The upward irradiances ($F^{\uparrow}_{\text{top}}$ and $F^{\uparrow}_{\text{base}}$) are relatively high. This is due to low clouds, which were present below the cirrus in the measurement area during the selected measurement period. In case of an atmosphere without clouds in between the cirrus and the ocean surface (dashed line), lower upward irradiance data have been measured. Due to the high altitude, about 9.2 km, no water vapor absorption bands are revealed in the near infrared spectra as shown by the almost unaffected downward irradiance in both levels. Therefore, all absorption of solar radiation, measured in the downward irradiance below the cirrus, originates from the cirrus itself.

The upward radiation depends on the albedo of the Earth's surface and underlying clouds, as can be seen in enhanced values of upward irradiance. The absorption bands of liquid water at wavelengths of 1140 nm or 1400 nm are obvious in the spectra. Furthermore, the irradiances F^{\uparrow} at both altitudes are similar. In comparison to the bright surface the difference due to the cirrus is not significant.

4.2.2 Spectra of reflectivity, absorptivity, transmissivity

By measuring the spectral and collocated upward and downward irradiances at two altitudes the cloud optical layer properties of the cirrus layer are derived according the Eq. (1) – (3) are derived. Fig. 7 (b) shows the spectral transmissivity (red, see Eq. 2), reflectivity (black, see Eq. 1), absorptivity (green, see Eq. 3), and cloud top albedo (gray, see Eq. 5) in the visible and near infrared wavelength range according to the example in Fig. 7 (a). The error bars result from the Gaussian error propagation due to uncertainties of calibration, of deviations from the ideal cosine angular sensor response correction, dark current, and signal to noise ratio. The resulting percentage errors range between 5 % and 6 % with higher values for the near infrared wavelength range.

As cirrus clouds are optically thin, the transmissivity dominates over the entire spectral range with high values between 88 % and almost 100 %. The reflectivity in Fig. 7 (b) shows very low values of not more than 3 %. This is due to the optically and vertically thin cirrus layer and a brighter water

cloud underneath. The effect of the low cloud is indicated by the cloud top albedo showing high values of about 40 % to 60 % in the depicted wavelength range.

The transmissivity shows a slightly negative spectral slope, absorptivity a positive trend, and the reflectivity shows no spectral trend. As the imaginary part of the refractive index is associated with the absorption coefficient, which increases with increasing wavelength, the measured absorptivity shows a spectral trend with a positive slope and values up to 12 % in the near infrared range, pointing out the importance of cirrus clouds in this wavelength range.

A time series of the cloud optical layer properties (at 1640 nm) is given in Fig. 8, with (a) transmissivity, (b) absorptivity, and (c) reflectivity, for the cirrus layer between 9.0 and 9.2 km altitude and a horizontal distance of 10.4 km. The cloud top albedo from below the aircraft (gray triangles), representing the cirrus and low-level cloud is plotted in (d).

The right panels (e)–(h) show the histograms for the respective cirrus properties in the left representing the variability during this flight part. As T , A , and R are cloud layer properties, the varying values are due to changing optical and microphysical properties of the cirrus. The layer properties of this thin cirrus show small variations, thus indicating small spatial heterogeneity of the optical layer properties. The transmissivity reveals the smallest variation between 0.890 and 0.925 (4 %). Absorptivity and reflectivity range between 0.078 and 0.098, and 0.001 – 0.008, resulting in a percentage difference of 21 % and 87 %, respectively, but still within the error bars.

The larger variability of R_{top} is explained by the changing reflectivity properties of the surface on the cloud top albedo. As the cirrus layer is optically thin, R_{top} from above the cirrus is strongly affected by the surface albedo and bright underlying water clouds resulting in R_{top} variations of about 11 % and significant differences in the absolute values.

5 Radiative transfer simulation

5.1 Model introduction

To compare the measurements with simulations and for a measurement – based quantification of the impact of different parameters, such as cloud particle shape and size on cirrus cloud optical layer properties, sensitivity studies with the one-dimensional (1D) radiative transfer model libRadtran (Mayer and Kylling, 2005) including the DISORT (DIScrete ORdinate Radiative Transfer) code by Stamnes et al. (2000) are performed. The observed cirrus layer is represented by varying cloud properties and the corresponding upward and downward irradiance at the top and the base of the cirrus are calculated to obtain the optical layer properties reflectivity, absorptivity, and transmissivity (according to Eq. (1) – (3)), and the cloud top albedo and radiative forcing (Eq. (5) – (6)).

The needed volumetric extinction coefficient $\langle b_{\text{ext},\lambda} \rangle$, single-scattering albedo $\langle \omega_{\lambda} \rangle$, and phase function $\langle p_{\lambda} \rangle$ are derived by combining calculated tables of single scattering properties by Yang et al. (2005) with a specific in situ measured number size distribution dN/dD (in cm^{-3}) from the CCP in-

stalled on AIRTOSS. The single scattering properties for individual particles (extinction coefficient
 260 $C_{\text{ext},\lambda}$, scattering coefficient $C_{\text{sca},\lambda}$, single-scattering albedo ω_λ , and phase function p_λ) with differ-
 ent particle radii are weighted with the number size distribution. The resulting spectral volumetric
 properties are used as input parameters for the radiative transfer simulations. The spectral volumetric
 extinction coefficient $\langle b_{\text{ext},\lambda} \rangle$ in units of km^{-1} was obtained by (see Wendisch et al., 2005):

$$\langle b_{\text{ext},\lambda} \rangle = \int C_{\text{ext},\lambda} \cdot \frac{dN}{dD} \cdot dD. \quad (7)$$

265 The boundaries of integration are defined by the size diameter range of the CCP. A similar algorithm
 was used to derive the spectral volumetric single-scattering albedo $\langle \omega_\lambda \rangle$ by calculating:

$$\langle \omega_\lambda \rangle = \frac{\int \omega_\lambda \cdot C_{\text{ext},\lambda} \cdot \frac{dN}{dD} \cdot dD}{\langle b_{\text{ext},\lambda} \rangle}. \quad (8)$$

Furthermore, the volumetric phase function $\langle p_\lambda \rangle$ is obtained by:

$$\langle p_\lambda \rangle = \frac{\int p \cdot C_{\text{sca},\lambda} \cdot \frac{dN}{dD} \cdot dD}{\int C_{\text{sca},\lambda} \cdot \frac{dN}{dD} \cdot dD}. \quad (9)$$

270 **5.2 Simulated spectra for individual cirrus layer**

To compare, in a first step, the measured cloud optical layer properties R , T , A , and cloud top albedo
 R_{top} with the simulated quantities, Fig. 10 (a) – (e) shows simulations of a cirrus layer between 9.0
 and 9.2 km altitude with different optical thicknesses. The input for the simulations includes a mea-
 275 sured number size distribution, shown in Fig. 9, which was measured during the AIRTOSS campaign
 and represents a typical cirrus. The ice crystal shape is assumed to be constant, further assuming a
 mixture of particle shapes according to Baum et al. (2005).

The cirrus optical thickness varies between 0.11 and 0.55. As expected, an increasing optical thick-
 ness leads to a decreased transmissivity T and increased reflectivity R , absorptivity A , and cloud top
 albedo R_{top} . The spectral trend shows pronounced effects for T and A in the near infrared wavelength
 280 range excluding the ranges of the water vapor absorption bands resulting in percentage differences of
 10 % and a factor of 5, respectively, between the optically thinnest and thickest cloud layer. The ab-
 sorptivity varies in the range of the ice particle absorption and causes a difference by up to a factor of
 5, whereas the cloud top albedo shows a similar difference of a factor of 5 in the wavelength range
 of water vapor absorption. According to the changes in the layer properties, the radiative forcing
 285 varies most between those cases while the absolute differences are small, varying between -0.006
 and $-0.033 \text{ W m}^{-2} \text{ nm}^{-1}$ (at 550 nm).

Comparing the measured (diamonds) and simulated (lines) spectral cloud optical layer properties, it
 can be seen, that there are visible discrepancies due to different possible input parameters such as
 optical thickness, ice crystal shape, and properties of the underlying surface.

290 As a cirrus cloud of 200 m vertical extent is not a typical one, for further sensitivity studies a cirrus
 between 6.7 and 8.5 km altitude is assumed, according to the measurement case of 30 August 2013

(see Fig. 5). The implemented number size distribution (Fig. 9) and the assumption of a mixture of shapes, described by Baum et al. (2005), results in an cirrus optical thickness of 1, representing a typical cirrus cloud.

295 To investigate the effect of different ice crystal shapes (see Fig. 11), a fixed number size distribution is combined with different shape assumptions: Solid Column, Column – 8 Elements, Plate, Plate 10 – Elements, Solid Bullet Rosette, Droxtal, and a mixture of 30 % Plates (10 Elements), 30 % Hollow Bullet Rosettes, 20 % Plates, and 20 % Hollow Columns, similar to the mixture according to Baum et al. (2005). The multi–component ice crystals, such as Column – 8 Elements, are aggregates consisting of their respective number of crystals. The different crystal shapes are introduced by Yang et al. (2013). The ice crystal roughness is set to smooth, see Baum et al. (2010).

Two approaches are investigated: (I) the number size distribution is constant (NSD, left panels), (II) the ice water content is constant (IWC, right panels). As the number size distribution is derived from in situ measurements, assuming a constant *IWC* is a more physical approach.

305 Fig. 11 shows the simulated (lines) spectral optical layer properties transmissivity T (a,e), reflectivity R (b,f), and absorptivity A (c,g) for those crystal shapes. Additionally, the simulated radiative forcing RF_{toa} (see Eq. 6) in (e,h) are represented. As reference case the shape Droxtal (red line) is used approximating spherical particles. Table 1 shows the resulting optical thicknesses assuming different shapes for the two approaches.

310 The results for approach I show, that varying ice crystal shape causes differences that are spectrally dependent, especially for absorptivity in the near infrared wavelength range between 1450 and 1800 nm, and 1900 and 2200 nm, where the imaginary part of the refractive index of ice reveals a maximum. This corresponds to an increased absorption coefficient and, therefore, a pronounced shape effect in this wavelength range. A similar spectral trend of the shape effect shows the transmissivity.

The percentage difference of transmissivity between the varying shapes and the reference case (Droxtals) ranges between 5 % and 50 %. The lowest differences show Solid Columns and Plates, whereas the mixture according to Baum et al. (2005) and Plates (10 Elements) show highest values.

320 The shape variability is more pronounced for reflectivity and absorptivity with differences of up to 80 % and a factor of 2 for Plates (10 Elements), respectively.

In relation to the highest values of reflectivity the corresponding radiative forcing for Solid Columns and Droxtals are strongest with -0.20 and $-0.18 \text{ W m}^{-2} \text{ nm}^{-1}$ (at 550 nm) and for Plates (10 Elements) and the mixture according to Baum et al. (2005) lowest with -0.05 and $-0.06 \text{ W m}^{-2} \text{ nm}^{-1}$ (550 nm), respectively, resulting in pronounced cooling effects for Droxtals and Solid Columns. This

325 leads to a difference in the radiative forcing of a factor of up to 4 assuming different shapes.

Assuming a constant IWC of 0.395 g m^{-3} (approach II) for varying ice crystal shapes means keeping the total volume of the cirrus cloud particles constant. This leads to the largest variabilities between Droxtals, approximating spheres, and crystal shapes with a large surface area, such as aggregates

of shapes or rosettes. For transmissivity and absorptivity the resulting differences are no more than 60 %. The largest differences (factor of 4) are obtained for the reflectivity as well as for radiative forcing by a factor of 6, due to the link between the total surface area of a cloud and its capability of reflection. In comparison with approach I the second scenario II shows significantly larger variabilities assuming different shapes for the cloud optical layer properties and radiative forcing.

5.3 Cirrus and underlying low-level cloud

Chang and Li (2005) reported an annual and global occurrence of high clouds of 52 – 61 % (ocean – land), from which 27 % to 29 % represent cases with low clouds underneath the cirrus. During the flights very often low clouds were observed, that is why the related effect of a low-level water cloud was investigated. Fig. 12 shows two cirrus cases, one with (black line) and one without (red line) a low-level water cloud. The cirrus is the same case as in Fig. 11, Approach I, assuming the mixture of shapes according to Baum et al. (2005). For the second case a water cloud ($\tau = 20$) was added between 1 km and 1.25 km altitude. The measurement example is the same as shown in Fig. 7. Adding a low-level cloud in the simulation leads to a higher transmissivity (up to 6 %) and lower reflectivity (up to 90 %) of the cirrus layer except in the wavelength ranges of the water vapor absorption bands. As the cloud top albedo is no cirrus layer property it shows the largest difference for the low-level cloud case, but a good agreement with the measurement case in the shortwave-infrared wavelength range.

For characterizing the effect of a low water cloud on the radiative forcing of the cirrus and the atmosphere's energy budget, a modified radiative forcing RF'_{Ci} is introduced:

$$RF'_{Ci} = RF_{Ci+low\ cloud} - RF_{low\ cloud} \quad (10)$$

$$RF'_{Ci} = F^{\uparrow}_{low\ cloud} - F^{\uparrow}_{Ci+low\ cloud}.$$

The resulting RF'_{Ci} is the difference between the case of a cirrus with underlying low water cloud and the case with the low cloud only (as Keil and Haywood (2003) applied for aerosol layers) at top of atmosphere.

RF'_{Ci} is shown in Fig. 12 (e) (black line) in contrast to the radiative forcing RF (see Eq. 6) of the same but single-layer cirrus (red line). It is noticeable that there is a sign changing effect on RF' with negative values for the visible spectral range and a positive radiative forcing in the near infrared range. This leads to an overestimation of the cooling effect of the cirrus with a percentage difference of about 80 % in the visible wavelength range and up to a factor of 2 in the near infrared range caused by the low-level cloud.

The results obtained in this paper are valid for the respective cloud cases. To evaluate the low-level cloud effect on the cirrus the properties of the low water cloud, such as optical thickness and cloud top height, have to be investigated, too. Therefore, Fig. 13 (a) and (b) show values of integrated cirrus radiative forcings (wavelength range: 300–2300 nm) with varying water cloud optical thickness

(a) and cloud top height (b). The cirrus is located between 6.7 km and 8.5 km altitude and consists
365 of the mixture of shapes according to Baum et al. (2005). The color code represents the changing
cirrus optical thickness.

In Fig.13 (a) the low-level cloud is located between 1 km and 1.25 km with an increasing optical
thickness from 5 to 60. In general, the cooling of the cirrus decreases with increasing optical thick-
ness of the low cloud resulting in an increasing influence of the low cloud on the upper lying cirrus.
370 This is due to the reflected radiation by the low cloud being available to interact with the cirrus layer
again. With higher water cloud optical thickness a saturating effect can be seen resulting in differ-
ences of 72 % to 83 %. Additionally, with increasing cirrus optical thickness the absolute difference
of RF increases from 10 W m^{-2} to 32 W m^{-2} .

In Fig.13 (b) the low water cloud has a constant optical thickness of 20, and a vertical thickness of
375 250 m with an increasing cloud top height from 1.25 to 7.25 km. Similar to Fig.13 (a) the cooling of
the cirrus decreases with increasing cloud top height of the low-level cloud. Here, the amount of the
reflected radiation by the low cloud, available in the cirrus level, depends on the vertical extension of
the atmosphere in between and its interaction with the transmitted (from cirrus) and reflected (from
water cloud) radiation. The trend of RF is similar to (a) with increasing cloud top height with a
380 resulting in lower differences of 20 % to 35 % and absolute values of not more than 8 W m^{-2} .

It is noticeable that the cloud optical thickness of the low cloud in comparison to the cloud top height
has a significant effect on the radiative forcing of the above lying cirrus.

6 Conclusions

Spectra of optical layer properties of cirrus have been derived from the first truly collocated airborne
385 radiation measurements in the framework of the AIRTOSS (AIrcraft TOWed Sensor Shuttle) project.
The radiation measurements are complemented by microphysical in-situ measurements and radia-
tive transfer simulations, based on the microphysical data.

Two field campaigns have taken place above the North Sea and the Baltic Sea in spring and late sum-
mer 2013. Collocated measurements by an aircraft (Learjet 35A) and the towed platform AIRTOSS,
390 released on a towing cable underneath the plane, are collected above, beneath and inside the cirrus.
For radiation measurements the straight flight legs with minor changes of pitch and roll movements
of the measurement platform are selected for detailed analysis.

Spectral upward and downward irradiances in the visible and near infrared wavelength range above
and below the cirrus have been measured to derive the spectral transmissivity, absorptivity, reflec-
395 tivity, and cloud top albedo of the observed cirrus layer. Irradiance spectra and a time series for a
straight flight leg of 30 August 2013 are analyzed. The resulting layer properties at one wavelength
in the near infrared (1640 nm) differ only slightly due to horizontal inhomogeneities and the influ-
ence of low-level clouds, but with an increased effect due to low clouds in the cloud top albedo with

varying values of up to 11 %.

400 The impact of varying ice crystal shape and cloud particle size distribution is studied with a 1D radiative transfer model in combination with volumetric extinction coefficient, single-scattering albedo, and phase function calculated from measured in situ size distributions and tables of ice crystal single-scattering properties. The results show the highest sensitivity in cloud optical layer properties for varying ice crystal shapes for the absorptivity with up to a factor of 2 with respect to the reference
405 case of nearly spherical shaped Droxtals. The respective cirrus radiative forcing differs by a factor of up to 4 with a stronger cooling effect for Droxtals. A similar effect is due to an additional low-level water cloud, as observed during the measurement flights, with a noticeable difference in the reflectivity of the above lying cirrus of up to a factor of 2 under multi-layer conditions. The radiative forcing of the cirrus layer may switch sign and shows positive values in the near infrared wavelength
410 range with a resulting difference of up to a factor of 2. It was found that if a low-level cloud is not considered the solar cooling of the cirrus is strongly overestimated. The variation of the low-level cloud properties cloud top height and optical thickness influences the cirrus radiative forcing, too, resulting in differences of 35 and 83 %, respectively.

The application of measured in situ microphysical properties as input of radiative transfer simulations did not accurately reproduce the measured cirrus optical layer properties. This is partly due
415 to a variety of possible shapes and mixtures of shapes, and influenced by a changing albedo. Further adjustment of the simulations can probably be used to optimize the agreement and derive more information on the particle properties. The effect of the low-level water cloud has to be further investigated by varying the property of the cirrus, such as shape, size, and height of the cloud base and
420 top. As the interaction of the cirrus with terrestrial radiation is the important factor for affecting the Earth's energy budget, radiative transfer calculations in the terrestrial wavelength range have to be investigated.

Acknowledgements. This study was supported by the Deutsche Forschungsgemeinschaft through Project "WE 1900/19-1, BO 1829/7-1". Additional funding on a similar level for the aircraft certification of AIRTOSS and
425 for conducting the campaign was provided by internal sources of the Particle Chemistry Department at the Max Planck Institute for Chemistry. We thank the pilots and crew of the Gesellschaft für Flugziieldarstellung (GFD) and enviscope GmbH for preparation and execution of the test and research flights, and the colleagues from Forschungszentrum Jülich and University of Warsaw for their support.

References

- 430 Baum, B. A., Yang, P., Heymsfield, A. J., Platnick, S., King, M. D., Hu, Y. X., and Bedka, S. T.: Bulk scattering properties for the remote sensing of ice clouds. Part II: Narrowband models, *J. Appl. Meteor.*, 44, 1896–1911, 2005.
- Baum, B. A., Yang, P., Hu, Y. X., and Feng, Q. A.: The impact of ice particle roughness on the scattering phase matrix RID B-7670-2011 RID B-4590-2011, *J. Quant. Spectrosc. Radiat. Transfer*, 111, 2534–2549, doi:10.1016/j.jqsrt.2010.07.008, 2010.
- 435 Bierwirth, E., Wendisch, M., Ehrlich, A., Heese, B., Tesche, M., Althausen, D., Schladitz, A., Müller, D., Otto, S., Trautmann, T., Dinter, T., von Hoyningen-Huene, W., and Kahn, R.: Spectral surface albedo over Morocco and its impact on the radiative forcing of Saharan dust, *Tellus*, 61B, 252–269, 2009.
- Chang, F.-L., Li, Z.: A Near-Global Climatology of Single-Layer and Overlapped Clouds and Their Optical Properties Retrieved from Terra/MODIS Data Using a New Algorithm, *J. of Climate*, 18, 4752–4771, 2005.
- 440 Eichler, H., Ehrlich, A., Wendisch, M., Mioche, G., Gayet, J.-F., Wirth, M., Emde, C., and Minikin, A.: Influence of ice crystal shape on retrieval of cirrus optical thickness and effective radius: A case study, *J. Geophys. Res.*, 114, D19203, doi:doi:10.1029/2009JD012215, 2009.
- Field, P. R., Wood, R., Brown, P. R. A., Kaye, P. H., Hirst, E., Greenaway, R., and Smith, J. A.: Ice particle interarrival times measured with a fast FSSP, *J. Atmos. Oceanic Technol.*, 20, 249–261, 2003.
- 445 Field, P. R., Heymsfield, A., and Bansemer, A.: Shattering and particle interarrival times measured by Optical Array Probes in ice clouds, *J. Atmos. Oceanic Technol.*, 23, 1357–1370, 2006.
- Francis, P., Hignett, P., and Macke, A.: The retrieval of cirrus cloud properties from aircraft multi-spectral reflectance measurements during EUCREX '93, *Quart. J. Roy. Meteor. Soc.*, 124, 1273–1291, 1998.
- 450 Frey, W., Eichler, H., de Reus, M., Maser, R., Wendisch, M., and Borrmann, S.: A new airborne tandem platform for collocated measurements of microphysical cloud and radiation properties, *Atmos. Meas. Tech.*, 2, 147–158, 2009.
- Gayet, J. F., Auriol, F., Minikin, A., Strom, J., Seifert, M., Krejci, R., Petzold, A., Febvre, G., and Schumann, U.: Quantitative measurement of the microphysical and optical properties of cirrus clouds with four different in situ probes: Evidence of small ice crystals, *Geophys. Res. Lett.*, 29, 83-1 – 83-4, doi:10.1029/2001GL014342, 2002.
- 455 Henrich, F., Siebert, H., Jäkel, E., Shaw, R. A., and Wendisch, M.: Collocated measurements of boundary-layer cloud microphysical and radiative properties and comparison with satellite retrievals, *J. Geophys. Res.*, 115, D24 214, doi:10.1029/2010JD013930, 2010.
- 460 IPCC: Climate Change 2013: The Physical Science Basis, Cambridge University Press, Cambridge, United Kingdom and New York, NY, USA, 2013.
- Keil, A. and Haywood, J. M.: Solar radiative forcing by biomass burning aerosol particles during SAFARI 2000: A case study based on measured aerosol and cloud properties, *J. Geophys. Res.*, 108, 8467, doi:10.1029/2002JD002315, 2003.
- 465 Klingebiel, M., de Lozar, A., Molleker, S., Weigel, R., Roth, A., Schmidt, L., Meyer, J., A., E., Neuber, R., M., W., and Borrmann, S.: Arctic low-level boundary layer clouds: in situ measurements and simulations of mono- and bimodal supercooled droplet size distributions at the top layer liquid phase cloud, *Atm. Chem. Phys.*, 15, 617–631, 2015.

- Korolev, A. V., Emery, E. F., Strapp, J. W., Cober, S. G., and Isaac, G. A.: Quantification of the Effects of Shattering on Airborne Ice Particle Measurements, *J. Atmos. Ocean Technol.*, 30, 2527–2553, 2013.
- Liou, K.-N.: Influence of cirrus clouds on weather and climate processes: A global perspective, *Mon. Wea. Rev.*, 114, 1167–1199, 1986.
- Lynch, K., Sassen, K., Starr, D., Stephens, G., Heymsfield, A., Liou, K.-N., Minnis, P., and Platt, C.: *Cirrus*, Oxford University Press, New York, 2002.
- 475 Mayer, B. and Kylling, A.: Technical note: The *libRadtran* software package for radiative transfer calculations - description and examples of use, *Atmos. Chem. Phys.*, 5, 1855–1877, 2005.
- McFarquhar, G. M., Um, J., Freer, M., Baumgardner, D., Kok, G. L., and Mace, G.: Importance of small ice crystals to cirrus properties: Observations from the Tropical Warm Pool International Cloud Experiment (TWP-ICE), *Geophys. Res. Lett.*, 34, L13803, doi:10.1029/2007GL029865, 2007.
- 480 Müller, S., Hoor, P., Berkes, F., Bozem, H., Klingebiel, M., Reutter, P., Smit, H. G. J., Wendisch, M., Spichtinger, P., and Borrmann, S.: In-situ detection of stratosphere-troposphere-exchange of cirrus particles in the mid-latitudes, *Geophys. Res. Lett.*, 42, doi:10.1002/2014GL062556, 2015.
- Pilewskie, P. and Valero, F. P. J.: Radiative effects of the smoke clouds from the Kuwait oil fires, *J. Geophys. Res.*, 97, 14 541–14 544, 1992.
- 485 Schlimme, I., Macke, A., and Reichardt, J.: The impact of ice crystal shapes, size distributions, and spatial structures of cirrus clouds on solar radiative fluxes, *J. Atmos. Sci.*, 62, 2.274–2.283, 2005.
- Stamnes, K., Tsay, S.-C., Wiscombe, W., and Laszlo, I.: DISORT, a General-Purpose Fortran Program for Discrete-Ordinate-Method Radiative Transfer in Scattering and Emitting Layered Media: Documentation of Methodology, Tech. rep., Dept. of Physics and Engineering Physics, Stevens Institute of Technology, Hoboken, NJ 07030, 2000.
- 490 Wendisch, M. and Brenguier, J.-L.: *Airborne Measurements for Environmental Research – Methods and Instruments*, Wiley–VCH Verlag GmbH & Co. KGaA, Weinheim, Germany, Weinheim, Germany, ISBN: 978-3-527-40996-9, 2013.
- Wendisch, M., Müller, D., Schell, D., and Heintzenberg, J.: An airborne spectral albedometer with active horizontal stabilization, *J. Atmos. Oceanic Technol.*, 18, 1856–1866, 2001.
- 495 Wendisch, M., Pilewskie, P., Pommier, J., Howard, S., Yang, P., Heymsfield, A. J., Schmitt, C. G., Baumgardner, D., and Mayer, B.: Impact of cirrus crystal shape on solar spectral irradiance: A case study for subtropical cirrus, *J. Geophys. Res.*, 110, D03 202, doi:10.1029/2004JD005294, 2005.
- Wendisch, M., Yang, P., and Pilewskie, P.: Effects of ice crystal habit on thermal infrared radiative properties and forcing of cirrus, *J. Geophys. Res.*, 112, D03 202, doi:10.1029/2006JD007899, 2007.
- 500 Werner, F., Siebert, H., Pilewskie, P., Schmeissner, T., Shaw, R. A., and Wendisch, M.: New airborne retrieval approach for trade wind cumulus properties under overlying cirrus, *J. Geophys. Res.*, 118, 3634–3649, doi:10.1002/jgrd.50334, <http://dx.doi.org/10.1002/jgrd.50334>, 2013.
- Werner, F., Ditas, F., Siebert, H., Simmel, M., Wehner, B., Pilewskie, P., Schmeissner, T., Shaw, R. A., Hartmann, S., Wex, H., Roberts, G. C., and Wendisch, M.: Twomey effect observed from collocated microphysical and remote sensing measurements over shallow cumulus, *J. Geophys. Res.*, 119, 1534–1545, doi:10.1002/2013JD020131, <http://dx.doi.org/10.1002/2013JD020131>, 2014.
- 505

- Wylie, D., Menzel, W., Woolf, H., and Strabala, K.: Four years of global cirrus cloud statistics using HIRS, *J. Climate*, 7, 1972–1986, 1994.
- 510 Yang, P., Wei, H. L., Huang, H. L., Baum, B. A., Hu, Y. X., Kattawar, G. W., Mishchenko, M. I., and Fu, Q.: Scattering and absorption property database for nonspherical ice particles in the near- through far-infrared spectral region, *Appl. Opt.*, 44, 5512–5523, 2005.
- Yang, P., Bi, L., Baum, B. A., Liou, K. N., Kattawar, G. W., Mishchenko, M. I., and Cole, B.: Spectrally consistent scattering, absorption, and polarization properties of atmospheric ice crystals at wavelengths from 0.2 to 100
- 515 μm , *J. Atmos. Sci.*, 70, 330–347, 2013.
- Zhang, Y., Macke, A., and Albers, F.: Effect of crystal size spectrum and crystal shape on stratiform cirrus radiative forcing, *Atmos. Res.*, 52, 59–75, 1999.



Figure 1. Photo from the Learjet 35A with towed AIRcraft TOWed Sensor Shuttle. The picture was taken during a test flight from a second aircraft.

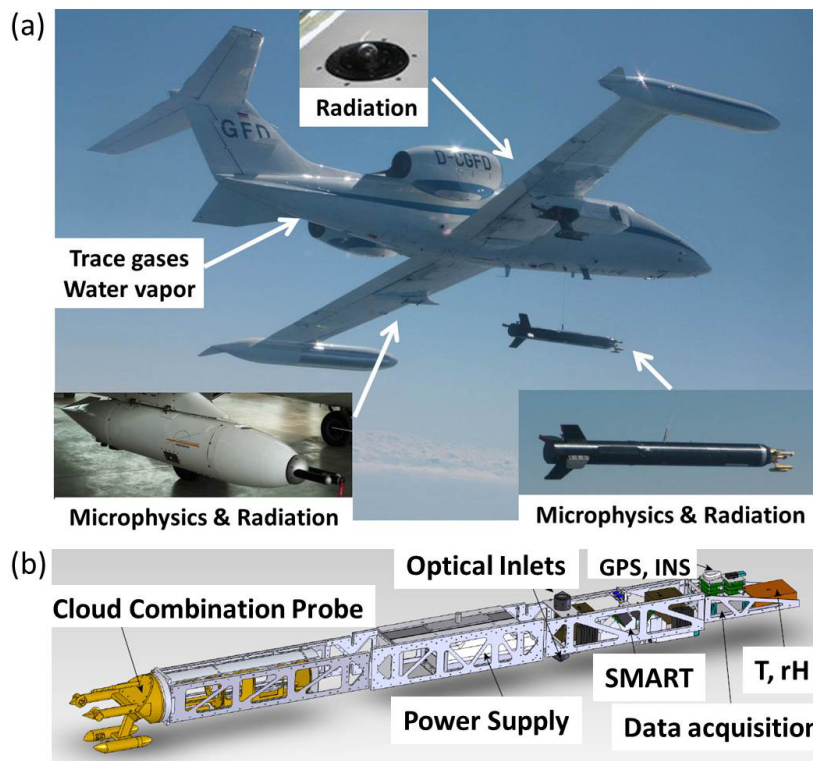


Figure 2. (a) Assembly of the research aircraft Learjet 35A, the towed AIRTOSS, and the wing pod containing instruments measuring radiation, microphysical parameter, water vapor, and trace gases. (b) Sketch of the AIRTOSS setup.

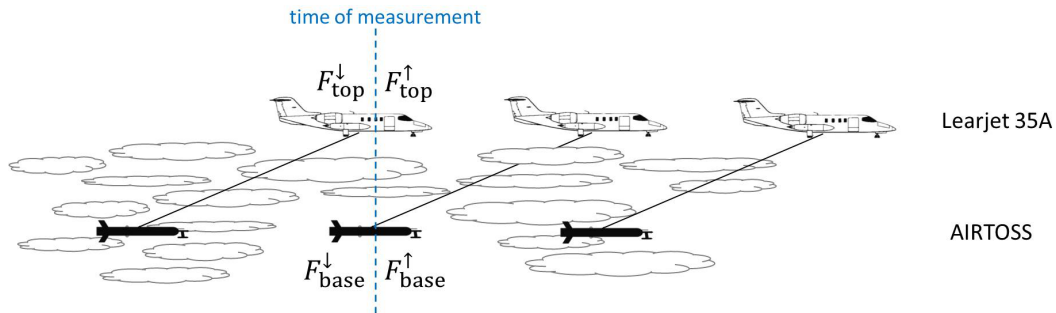


Figure 3. Schematic sketch of measurement setup to measure collocated upward ($F_{\text{top}}^{\uparrow}$) and downward ($F_{\text{top}}^{\downarrow}$) irradiance at two altitudes (base, top).

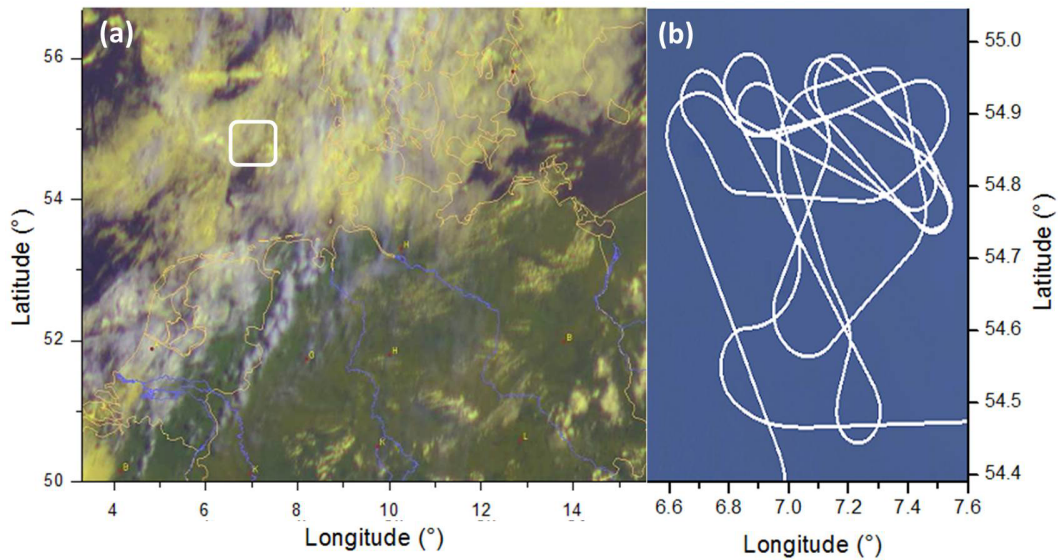


Figure 4. (a) Composite satellite image of the cloud situation on 30 August 2013 at 9:45 UTC showing cirrus (white) above yellow colored lower water clouds (Deutscher Wetterdienst / EUMETSAT). In (b) the flight track of the measuring flight in the restricted area (white box in (a)) above the North Sea near the island of Helgoland, North Germany, is shown.

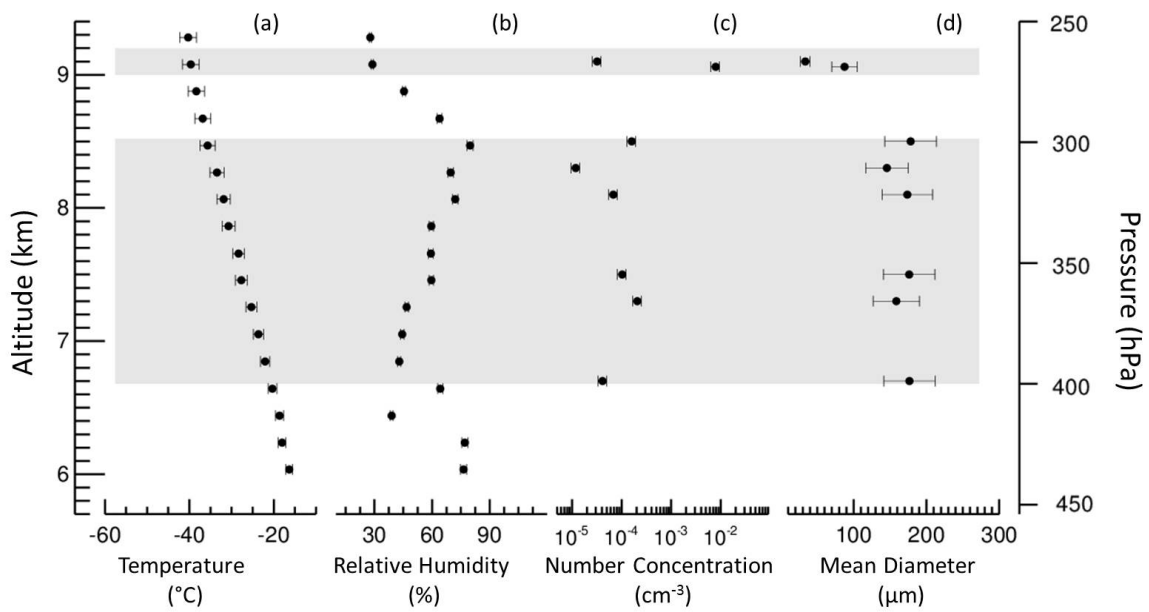


Figure 5. Vertical profiles of (a) temperature, (b) relative humidity, measured on the Learjet 35A, (c) number concentration, and (d) mean diameter, derived by CIPg on AIRTOSS, from the flight of 30 August 2013. The bars show the corresponding measurement uncertainties. The gray area indicates the vertical extent of the cirrus layer.

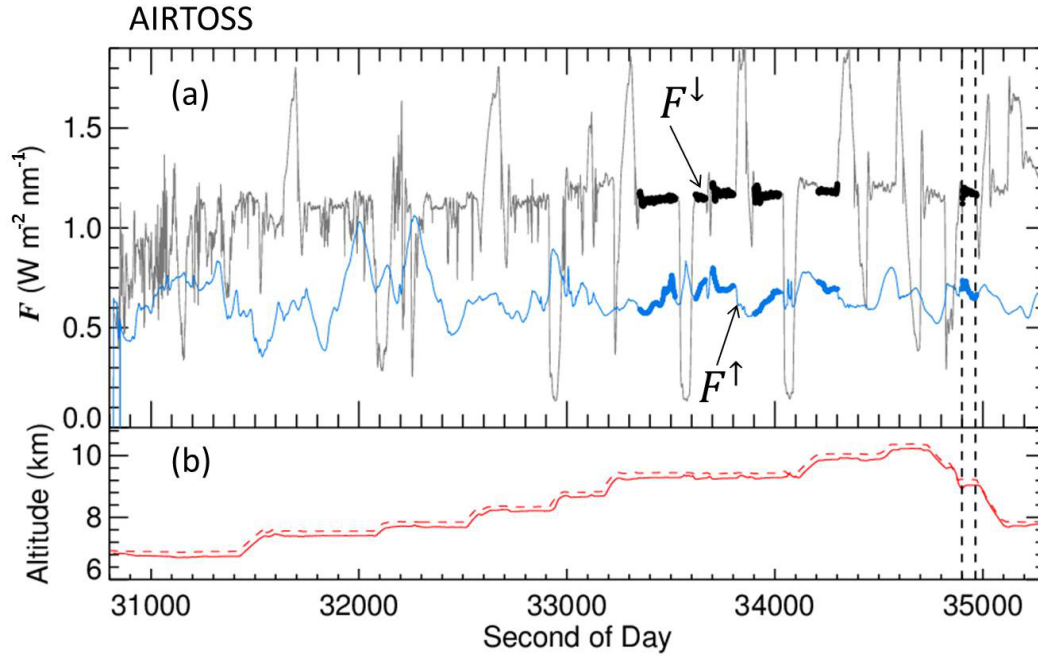


Figure 6. (a) Time series of downward (gray) and upward (light blue) irradiance F ($\text{W m}^{-2} \text{nm}^{-1}$) measured on AIRTOSS at one wavelength (550 nm) from the flight of 30 August 2013. The thickened line periods mark the measuring points at straight flight legs. The red lines in (b) show the altitude of AIRTOSS (solid) and Learjet (dashed). The vertical dashed line marks the measurement example in Fig. 7.

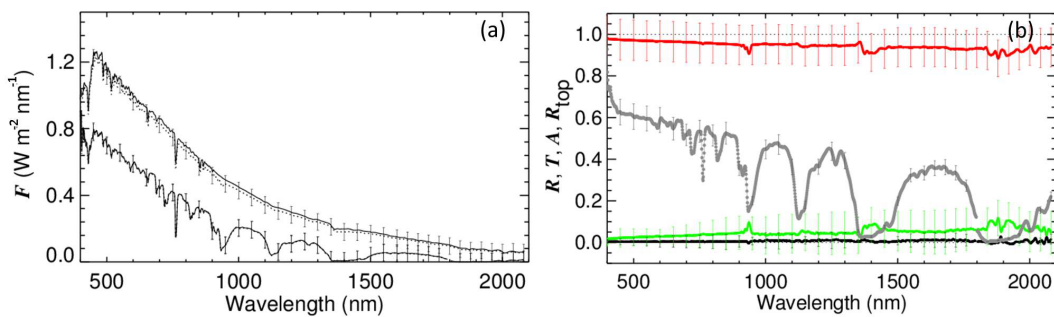


Figure 7. (a) shows measured spectral downward and upward irradiance F from the aircraft above the cloud layer (solid lines) and AIRTOSS below the cloud layer (dotted lines) at the time, indicated by the vertical dashed line in Fig. 6. $F_{\text{top}}^\downarrow$ is simulated. (b) shows spectral reflectivity (black), transmissivity (red), absorptivity (green), and cloud top albedo (gray) according to irradiance in (a). The vertical bars indicate the systematic errors due to measurement uncertainties.

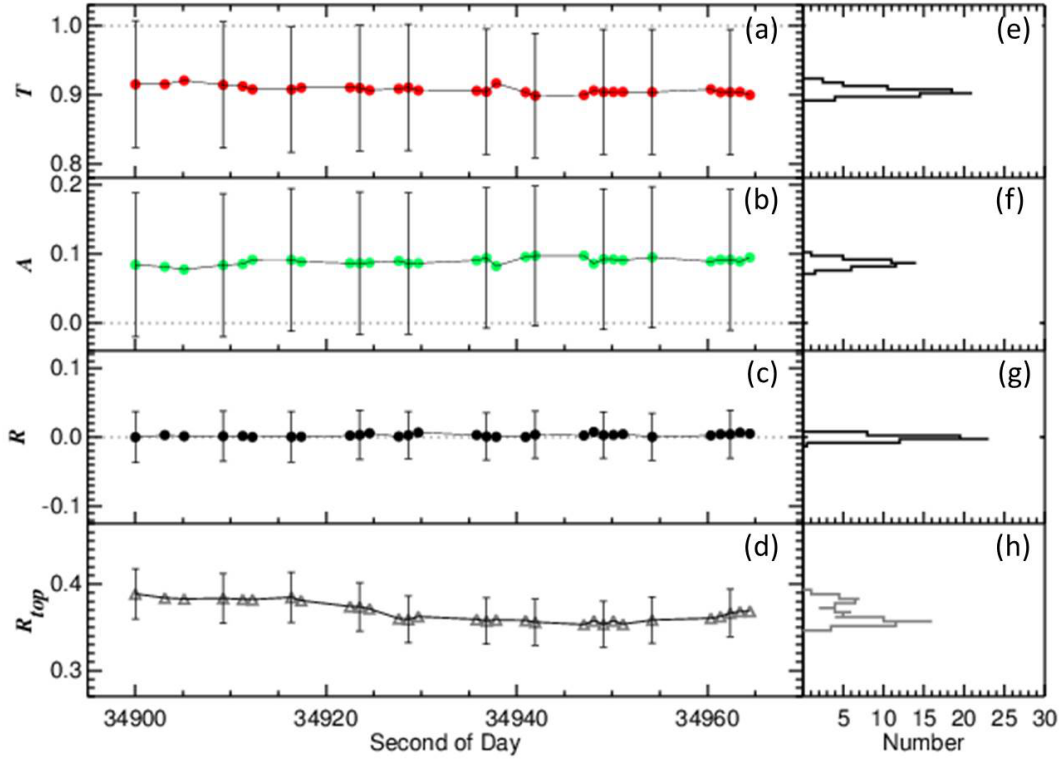


Figure 8. Shown are time series of (a) transmissivity, (b) absorptivity, and (c) reflectivity (at 1640 nm) for the cirrus layer between 9.0 and 9.2 km altitude on 30 August 2013. The associated cloud top albedo is plotted in (d). The vertical bars represent the errors due to measurement uncertainties. (e) – (h) show the histograms, respectively.

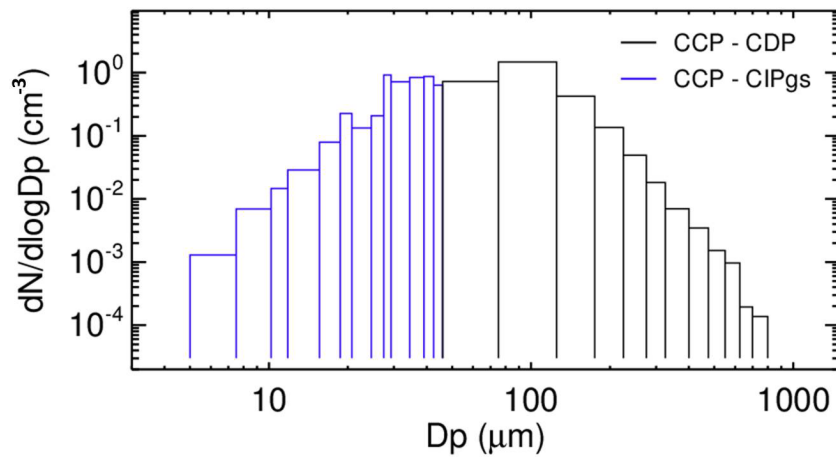


Figure 9. Number size distribution of a cirrus cloud, measured during the AIRTOSS campaign by the Cloud Combination Probe at the AIRcraft TOWed Sensor Shuttle.

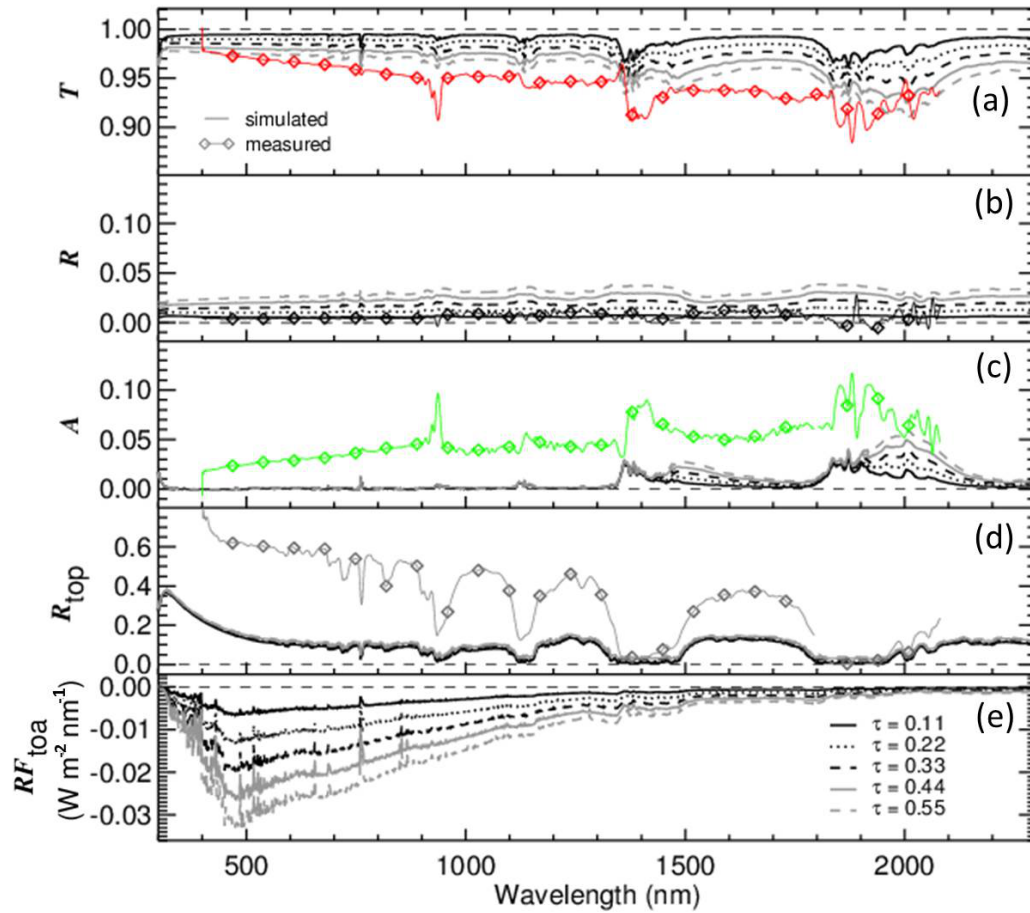


Figure 10. The lines show simulated, spectral (a) transmissivity, (b) reflectivity, and (c) absorptivity of a cirrus layer between 9 km and 9.2 km altitude. (e) are the radiative forcings at TOA, respectively. The simulations are based on a measured number size distribution assuming the mixture of shapes according Baum et al. (2005). Inserted is the measurement case (diamonds) from Fig.7.

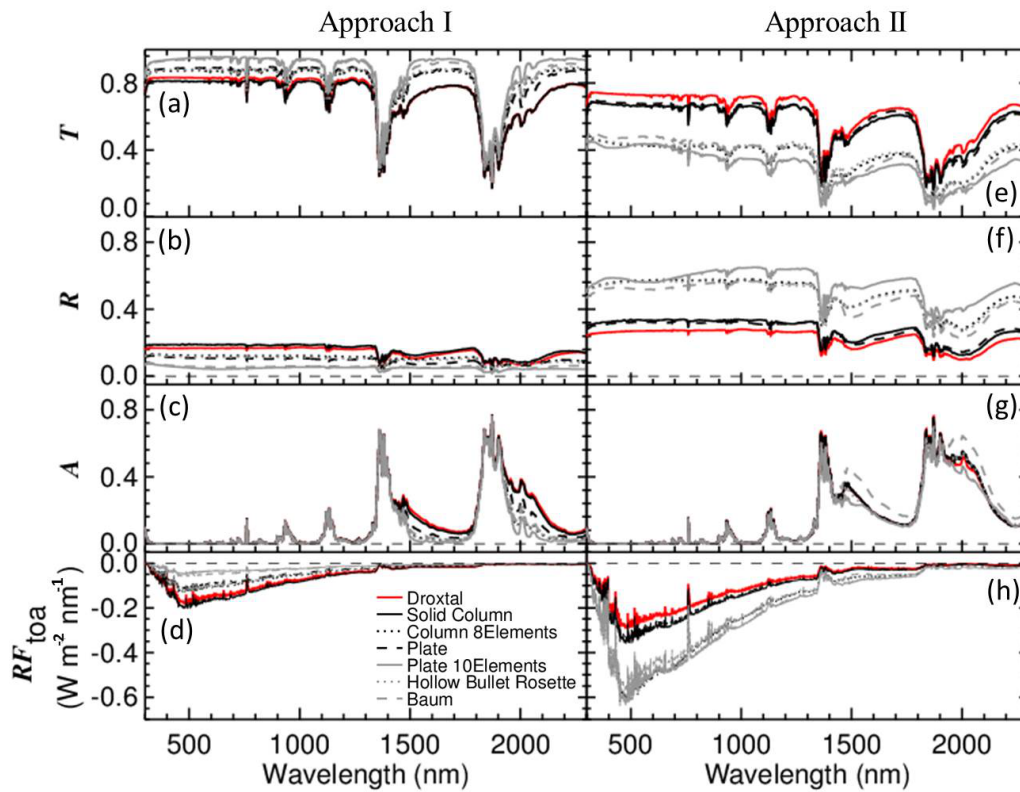


Figure 11. Shown are spectral (a,e) transmissivity, (b,f) reflectivity, and (c,g) absorptivity of a cirrus layer between 6.7 and 8.5 km altitude. (e,h) are the radiative forcings at TOA, respectively. The simulations are based on a measured number size distribution assuming different ice particle shapes. The two panels indicate two conditions: constant number size distribution (Approach I) and constant ice water content (Approach II).

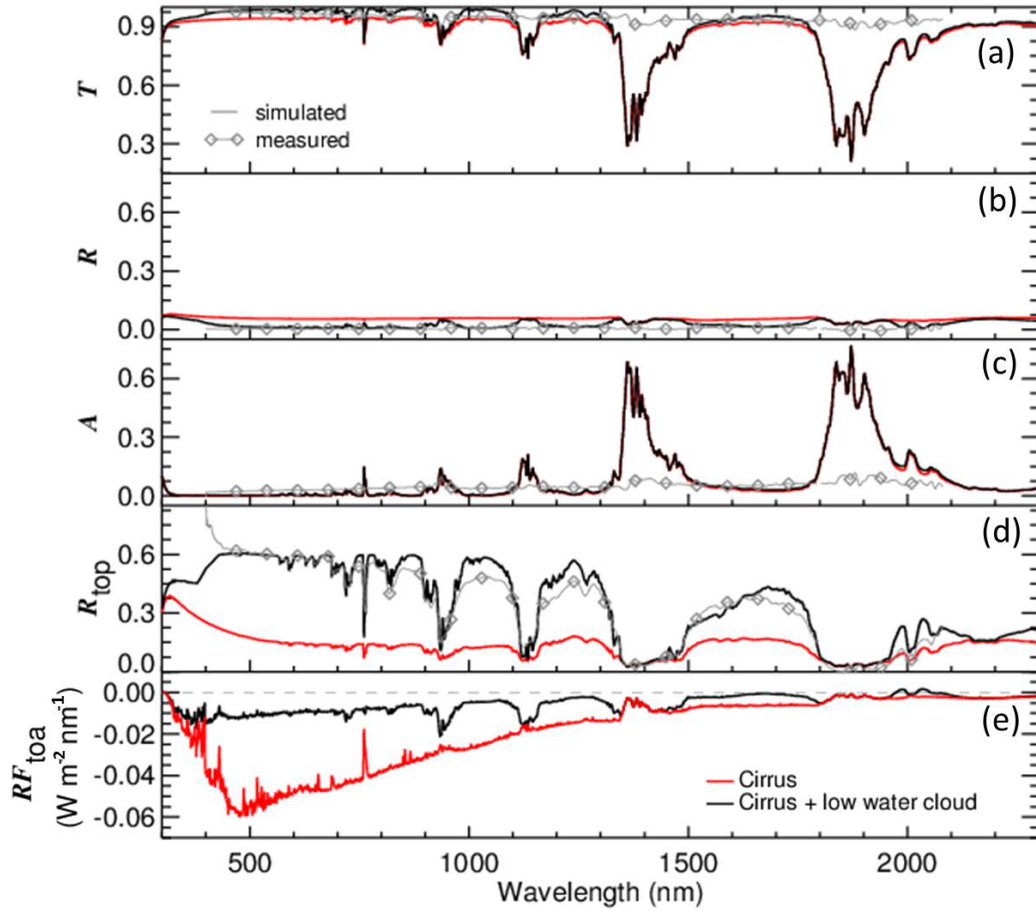


Figure 12. Same as Fig.10 assuming the mixture according to Baum et al. (2005) between 6.7 and 8.5 km altitude ($\tau_{\text{Cirrus}} = 1$). An additional low water cloud with $\tau = 20$ is included between 1.0 and 1.25 km altitude. Inserted is the measurement case (gray diamonds).

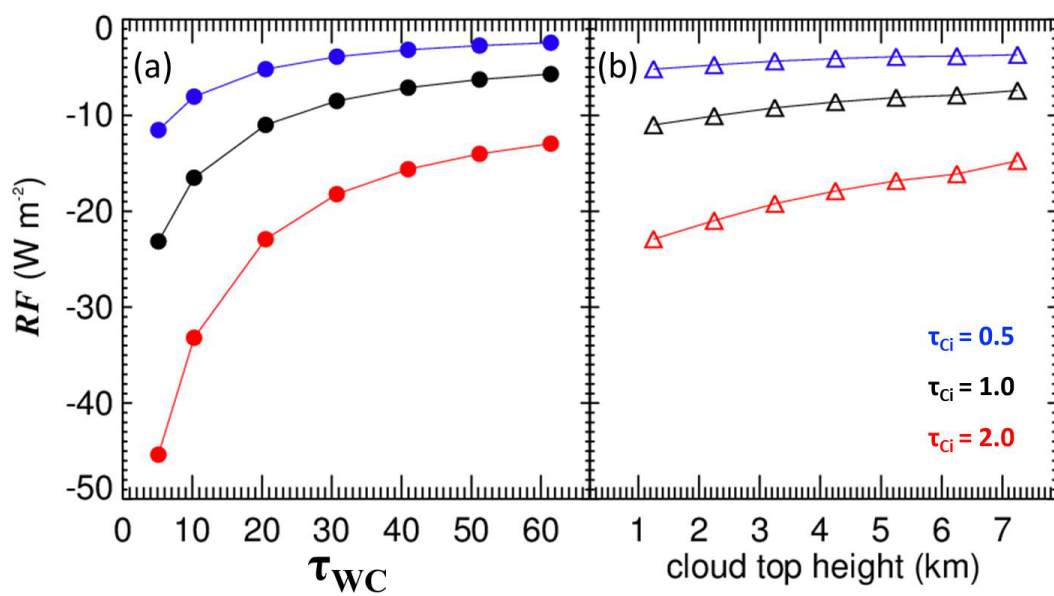


Figure 13. Integrated values of cirrus radiative forcing when a low water cloud is present. The optical thickness (left panel), and the top height (right panel) of the water cloud are varied. The colors indicate a different cirrus optical thickness.

Table 1. Shown are the optical thicknesses for a cirrus between 6.7 km and 8.5 km altitude assuming different ice crystal shapes for Approach I (constant number size distribution) and Approach II (constant ice water content).

	Approach I	Approach II
Droxtal	1.49	2.68
Solid Column	1.50	3.20
Column 8 Elements	0.77	7.45
Plate	1.15	4.44
Plate 10 Elements	0.54	15.4
Hollow Bullet Rosette	0.97	9.52
Baum	1.00	5.09